Variable Eddington Factor and Radiating Slowly Rotating Bodies in General Relativity

F. Aguirre

Laboratorio de Física Teórica, Departamento de Física, Facultad de Ciencias, Universidad de Los Andes, Mérida 5101, Venezuela

aguirre@ula.ve

L. A. Núñez

Centro de Física Fundamental, Departamento de Física, Facultad de Ciencias, Universidad de Los Andes, Mérida 5101, Venezuela, and
Centro Nacional de Cálculo Científico Universidad de Los Andes (CeCalCULA)
Corporación Parque Tecnológico de Mérida, Mérida 5101, Venezuela

nunez@ula.ve

T. Soldovieri

Laboratorio de Investigaciones de Física Teórica (LIFT), Departamento de Física, Facultad de Experimental de Ciencias, Universidad del Zulia, Maracaibo Zulia, Venezuela

tsoldovieri@luz.edu.ve

ABSTRACT

We present an extension to a previous work to study the collapse of a radiating, slow-rotating self-gravitating relativistic configuration. In order to simulate dissipation effects due to the transfer of photons and/or neutrinos within the matter configuration, we introduce the flux factor, the variable Eddington factor and a closure relation between them. Rotation in General Relativity is considered in the slow rotation approximation, i.e. tangential velocity of every fluid element is much less than the speed of light and the centrifugal forces are little compared with the gravitational ones. Solutions are properly matched, up to the first order in the Kerr parameter, to the exterior Kerr-Vaidya metric and the evolution of the physical variables are obtained inside the matter configuration. To illustrate the method we work out three models with different equations of state and several closure relations. We have found that, for the closure relations considered, the matching conditions implies that a total diffusion regime can not be attained at the surface of the configuration. It has also been obtained that the eccentricity at the surface of radiating configurations is greater for models near the diffusion approximation

than for those in the free streaming out limit. At least for the static "seed" equations of state considered, the simulation we performed show that these models have differential rotation and that the more diffusive the model is, the slower it rotates.

Subject headings: stars: rotation — stars: neutron — radiative transfer — equation of state — gravitation — relativity

1. Introduction

Compact objects are one of the most fascinating objects known in our Universe. White dwarfs, neutron stars, quark stars, hyperon stars, hybrid stars and magnetars are thought to be relics from most of the cores of luminous stars which we believe to be born in supernova explosions. Core collapses are triggered by the implosion of the inner nucleus of a massive star ($M_\star \sim 8 - 20 M_\odot$) when its mass is in the limit of Chandrashekar ($M_{core} \sim 1.4 M_\odot$). During the implosion nearly all of an enormous gravitational binding energy ($(GM^2)/R \sim 5 \times 10^{53}$ ergs $\sim 0.2 Mc^2$) gained is stored as internal energy of a newly born, proto-neutron star (PNS) and its subsequent evolution is driven by neutrino diffusion which cools this new type of compact object. Temporal and spectral characteristics of the neutrino emission depend on the rate at which they diffuse through the imploded PNS which, at this early stage, would have a mean density several times the standard nuclear density, $\bar{\rho} \sim 3M/\left(4\pi R^3\right) \approx 7 \times 10^{14} g\ cm^{-3}$, with $\rho_0 \simeq 2. \times 10^{14} g\ cm^{-3}$. The core density reaches up to $(10 - 20)\rho_0$ during the cooling time $t_{cool} \sim 5$ to 10 s, while the PNS de-leptonizes by neutrino emission, cools, contracts and spin-ups to form the final ultradense compact object (Demianski 1985; Shapiro & Teukolsky 1983; Kippenhahn & Weigert 1990; Glendening 2000).

There is a consensus that the above standard scenario requires the description of General Relativity because of the formidable gravitational fields arising during these processes. These powerful gravitational fields strongly couple hydrodynamics and neutrino flows within rotating matter configurations (see Bruenn et al (2001) for a good historical survey of previous works done at various levels on the problem of coupling the General Relativity, hydrodynamics, and radiation transport in spherical symmetry). Unfortunately despite a considerable effort that is been carried out by a significant group of people and institutions, presently we do not have any self-consistent model either analytical or numerical that includes all of those components in full details.

Although an exterior metric of a rapidly rotating neutron agrees with the corresponding Kerr metric only to lowest order in the rotational velocity (Hartle & Thorne 1969), there have been many attempts to find a closed interior solution which matches smoothly to the gravitational field outside a rotating source (see (Stergioulas 2003; Font 2003; Lorimer 2001) and references therein). In general these attempts have proved to be unsuccessful essentially because the considerable mathematical complexity in solving the Einstein equations (Chinea & Gonzalez-Romero 1993). It is only very recently, that there has been reported some progress in the analytical approach (Manko et al 2000) which approximately match numerical solutions for rapidly rotating neutron stars (Berti &

Stergioulas 2004; Berti et al 2004) and has been used in studies of energy release (Sibgatullin & Sunyaev 2000; Siebel et al 2003). Recent numerical research has also considerably advanced our understanding of rotating relativistic stars (Dimmelmeier et al 2002). There now exist several independent numerical codes for obtaining accurate models of rotating neutron stars in full General Relativity (see Stergioulas (2003) and Font (2003) for a good review on this subject). We can particularly mention a 3D general-relativistic hydrodynamics code (GR Astro) written for the NASA Neutron Star Grand Challenge Project (NASAGC 2000; GRAstro3D 2000) and built from the Cactus Computational Toolkit (Cactus 2000).

Simulations which include better microphysics in the form of realistic nuclear equations of state or neutrino transport have either been confined to spherical symmetry or restricted to newtonian gravity. Today, all available models analytical/numerical resembling some pieces of truth, demonstrate remarkable sensitivities to different physical aspects of the problem, in particular the treatment of neutrino transport and neutrino-matter interactions, the properties of the nuclear equation of state (EoS), multi-dimensional hydrodynamical processes, effects of rotation and general relativity. It is worth mentioning that is just recently, when it has become possible to obtain spherically symmetric general relativistic hydrodynamical core-collapse, treating the time and energy dependent neutrino transport in hydrodynamical simulations by considering a Boltzmann solver for the neutrino transport (Liebendorfer et al 2001, 2002), implementing multigroup flux-limited diffusion to Lagrangian Relativistic Hydrodynamics (Bruenn et al 2001) or assuming the variable Eddington factor method to deal with the integro-differential character of the Boltzmann equation (Rampp & Janka 2002).

The present paper lies in between the traditional analytical and the emerging numerical descriptions of gravitational collapse. It follows a seminumerical approach which considers, under some general and reasonable physical assumptions, the evolution of a general relativistic rotating and radiating matter configurations. The rationale behind this work is twofold, first it seems useful to consider relatively simple nonstatic models to analyze some essential features of realistic situations that purely numerical solutions could hinder. Particularly, we will focus on the influence upon the evolution of matter configurations of the dissipation mechanism due to the emission of photons/neutrinos. Secondly it could be helpful for the evolving numerical codes to have testbed arena including General Relativity, rotation, dissipation and plausible EoS.

The approach we follow to solve the Einstein Equations starts from heuristic assumptions relating density, pressure, radial matter velocity and choosing a known interior (analytical) static spherically symmetric (considered as "seed") solution to the Tolman-Oppenheimer-Volkov equation. This scheme transforms the Einstein partial differential equations into a system of ordinary differential equations for quantities evaluated at surfaces whose numerical solution, allows the modelling of the dynamics of the configuration. This method is an extension of the so called HJR (Herrera et al 1980), which has been successfully applied to a variety of astrophysical scenarios (see Herrera & Núñez (1990) and Hernández et al (1998) and references therein) and which has been recently revisited (Barreto et al 2002; Herrera et al 2002) in order to appreciate its intrinsic

worth.

We are going to consider the effects of rotation in General Relativity in the slow rotation approximation, i.e. up to the first order, thus we shall maintain only linear terms in the angular velocity of the local inertial frames. Thus, the effects of rotation are purely relativistic and manifest through the dragging of local inertial frames (Hartle 1967; Hartle & Thorne 1968). This is understandable if we recall that in the newtonian theory where the parameter measuring the "strength" of rotation (the ratio of centrifugal acceleration to gravity at the equator) is not linear in the angular velocity but proportional to the square of it. The slow rotation approximation has recently proved to be very reliable for most astrophysical applications (Berti et al 2004). This assumption is very sensible because it considers that the tangential velocity of every fluid element is much less than the speed of light and the centrifugal forces are little compared with the gravitational ones. It is worth mentioning that the continuity of the *first* and the *second fundamental* (g_{ij} and K_{ij}) forms across the matching surface are also fulfilled up to this order of approximation.

Conscious of the difficulties to cope with dissipation due to the emission of photons and/or neutrinos and, aware of the uncertainties of the microphysics when considering the interaction between radiation and ultradense matter, we extend a previous work (Herrera et al 1994) to study the collapse of a radiating, slow-rotating self-gravitating relativistic configuration by introducing a relation between the radiation energy flux density and the radiation energy density, i.e. the *flux factor,* $f = \mathcal{F}/\rho_R$, and the so called *variable Eddington factor,* $\chi = \mathcal{P}/\rho_R$, relating the radiation pressure and the radiation energy density, We have also include a closure relation between both quantities, i.e., $\chi = \chi(f)$. In the literature several closures have been introduced (see Levermore (1984) for a comprehensive review and Domínguez (1997), Pons et al (2000) and Smit et al (2000) for more recent references) and most of them are consistent with the hiperbolicity and causality required by a relativistic theory (Pons et al 2000).

With the above set of assumptions, i.e. seminumerical approach to solve the Einstein system, slow rotation approximation, and a particular closure relation between the flux and the variable Eddington factor, we shall explore the effect of dissipation on the evolution of the rotating radiating matter configuration. The outcomes from our simulations could represent rotating compact objects where the core rotates faster than the envelope. Therefore, the core can be supported by rapid rotation while the velocity of the fluid at the equator does not exceed the limit imposed by a fluid moving along a geodesic (the Kepler limit). Thus, differential rotation may play an important role for the stability of these remnants, since it can be very effective in increasing their maximum allowed mass. This effect was demonstrated in newtonian gravitation in (Ostriker et al 1966) and was recently found by Shapiro and collaborators for general relativistic configurations having a polytropic EoS (Baumgart et al 2000; Lyford et al 2002). For these rotating matter distribution we have found that boundary conditions imply that at the surface of the configuration, a total diffusion regime can not be attained. It has also been obtained that, with these coordinates, the eccentricity at the surface of radiating configurations, (up to first order) is greater for models near the diffusion limit approximation than for those in the free streaming out limit even though the

rotation of configurations with dissipation near the diffusion limit appears to be slower than those near the free streaming out limit. We noticed that, at least for the static "seed" equations of state considered, it seems that the lower the flux factor we have, the slower is the rotation of the configuration.

The plan for the present work is the following. The next section contains an outline of the general conventions, notation used, the metric, the structure of the energy tensor and the corresponding field equations. Section 3 is devoted to describe the variable Eddington factor, the closure relations and the limits for the radiation field. Junction conditions and their consequences are considered in Section 4. The method is sketched in Section 5. We work out the modelling, previously studied for the spherical (nonrotating) case in Section 6. Finally some comments and conclusions are included in 7.

2. Energy-Momentum Tensor and field equations

2.1. The metric

As in the previous work (Herrera et al 1994), let us consider a nonstatic, axially symmetric distribution of matter conformed by fluid and radiation where the exterior metric, in radiation coordinates(Bondi 1964), is the Kerr-Vaidya metric(Carmeli & Kaye 1977):

$$ds^2 = \left(1 - \frac{2m\,(u)\;\; r}{r^2+\alpha^2\cos^2\theta}\right)\mathrm{d}u^2 + 2\mathrm{d}u\mathrm{d}r - 2\alpha\sin^2\theta\mathrm{d}r\mathrm{d}\phi + 4\alpha\sin\theta^2\frac{m\,(u)\;\; r}{r^2+\alpha^2\cos^2\theta}\mathrm{d}u\mathrm{d}\phi$$
$$- (r^2+\alpha^2\cos^2\theta)\mathrm{d}\theta^2 - \sin^2\theta\left[r^2+\alpha^2+\frac{2m\,(u)\;\; r\;\alpha^2\sin^2\theta}{r^2+\alpha^2\cos^2\theta}\right]\mathrm{d}\phi^2\ . \tag{1}$$

Here, $m\,(u)$ is the total mass and α is the Kerr parameter representing angular momentum per unit mass in the weak field limit. It is worth mentioning at this point that the metric above is not a pure radiation solution and may be interpreted as such only asymptotically (González et al 1979). A pure rotating radiation solution may be found in reference (Kramer & Hahner 1995). However, as we shall show below although the interpretation of the Carmeli-Kaye metric in not completely clear, the model dependence of the considered effect is independent of the shape and the intensity of the emission pulse, and may be put in evidence even for a tiny radiated energy, $\Delta M_{rad} = 10^{-12}M(0)$, which for any practical purpose corresponds to the Kerr metric(Herrera et al 1994). The interior metric is written as (Herrera & Jimenez 1982)

$$ds^2 = e^{2\beta}\left\{\frac{V}{r}\mathrm{d}u^2 + 2\mathrm{d}u\mathrm{d}r\right\} - (r^2+\tilde{\alpha}^2\cos^2\theta)\mathrm{d}\theta^2 + 2\tilde{\alpha}e^{2\beta}\sin^2\theta\left\{1-\frac{V}{r}\right\}\mathrm{d}u\mathrm{d}\phi$$
$$- 2e^{2\beta}\tilde{\alpha}\sin^2\theta\mathrm{d}r\mathrm{d}\phi - \sin^2\theta\left\{r^2+\tilde{\alpha}^2+2\tilde{\alpha}^2\sin^2\theta\frac{V}{r}\right\}\mathrm{d}\phi^2. \tag{2}$$

In the above equations (1) and (2), $u = x^0$ is a time like coordinate, $r = x^1$ is the null coordinate and $\theta = x^2$ and $\phi = x^3$ are the usual angle coordinates. Local minkowskian coordinates (t, x, y, z) are related to Bondi radiation coordinates (u, r, θ, ϕ) by

$$\mathrm{d}t = e^{\beta}\left(\sqrt{\frac{V}{r}}\mathrm{d}u + \sqrt{\frac{r}{V}}\mathrm{d}r\right) + \widetilde{\alpha}\sin^2(\theta)\, e^{\beta}\left(\sqrt{\frac{r}{V}} - \sqrt{\frac{V}{r}}\right)\mathrm{d}\phi; \tag{3}$$

$$\mathrm{d}x = e^{\beta}\sqrt{\frac{r}{V}}\left(\mathrm{d}r + \widetilde{\alpha}\sin^2(\theta)\,\mathrm{d}\phi\right); \quad \mathrm{d}y = \sqrt{r^2 + \widetilde{\alpha}\cos^2(\theta)}\mathrm{d}\theta \tag{4}$$

$$\text{and} \quad \mathrm{d}z = \sin(\theta)\sqrt{r^2 + \widetilde{\alpha}\cos^2(\theta)}\mathrm{d}\phi. \tag{5}$$

The u-coordinate is the retarded time in flat space-time, therefore, u-constant surfaces are null cones open to the future. This last fact can be readily noticed from the relationships between the usual Schwarzschild coordinates, (T, R, Θ, Φ), and Bondi's radiation coordinates:

$$u = T - \int \frac{r}{V}\, dr, \quad \theta = \Theta, \quad r = R \quad \text{and} \quad \phi = \Phi\ , \tag{6}$$

which are valid, at least, on the surface of the configuration.

The Kerr parameter for the interior space-time (2) is denoted $\tilde{\alpha}$ and, for the present work it is relevant only (as well as α in eq. (1)) up to the *first order*. Notice that, in these coordinates, the $r = r_s = const$, represent surfaces that are not spheres but *oblate spheroids*, whose eccentricity depends upon the interior Kerr parameter $\tilde{\alpha}$ and is given by

$$e^2 = 1 - \frac{r_s^2}{r_s^2 + \tilde{\alpha}^2}\ . \tag{7}$$

Observe that this expression of eccentricity yielding the correct newtonian limit and corresponding to the natural definition in the context of metrics (1) and (2), is not invariantly defined .

The metric elements β and V in eq. (2), are functions of u, r and θ. A function $\tilde{m}(u, r, \theta)$ defined by

$$V = e^{2\beta}\left(r - \frac{2\tilde{m}(u, r, \theta)r^2}{r^2 + \tilde{\alpha}^2\cos^2\theta}\right)\ , \tag{8}$$

is the generalization, inside the distribution, of the "mass aspect" defined by Bondi and collaborators (Bondi et al 1962) and in the static limit coincides with the Schwarzschild mass.

2.2. Energy-Momentum Tensor

It is assumed that, for a local observer co-moving with a fluid having a velocity $\vec{\omega} = (\omega_x, 0, \omega_z)$, the space-time contains:

- an isotropic (pascalian) fluid represented by $\hat{T}_{\mu}^{M\ \nu} = diag\,(\rho, -P, -P, -P)$. Where ρ is the energy density and $P = P_r$ the radial pressure. Although the perfect pascalian fluid assumption (i.e. $P_r = P_\perp$) is supported by solid observational and theoretical grounds, an increasing amount of theoretical evidence strongly suggests that, for certain density ranges, a variety of very interesting physical phenomena may take place giving rise to local anisotropy (see (Herrera & Santos 1997) and references therein).

- a radiation field of specific intensity $\mathbf{I}(r, t; \vec{n}, \nu)$ given through

$$\mathrm{d}\mathcal{E} = \mathbf{I}(r, t; \vec{n}, \nu)\mathrm{d}S\ \cos\varphi\ \mathrm{d}\Theta\ \mathrm{d}\upsilon\ \mathrm{d}t, \tag{9}$$

  with φ the angle between $\vec{n}$ and the normal to $\mathrm{d}S$ and where $\mathrm{d}\mathcal{E}$ is defined as the energy transported by a radiation of frequencies $(\nu, \nu + \mathrm{d}\upsilon)$ in time $\mathrm{d}t$, crossing a surface element $\mathrm{d}S$, through the solid angle around $\vec{n}$, i.e. $\mathrm{d}\Theta \equiv \sin\theta \mathrm{d}\theta\mathrm{d}\psi \equiv -\mathrm{d}\mu\mathrm{d}\psi$.
  As in classical radiative transfer theory, for a planar geometry the moments of $\mathbf{I}(r, t; \vec{n}, \nu)$ can be written as (Lindquist 1966; Mihalas & Mihalas 1984; Rezzolla & Miller 1994)

$$\rho_R = \frac{1}{2}\int_0^\infty d\nu \quad \int_1^{-1} d\mu \quad \mathbf{I}(r, t; \vec{n}, \nu), \qquad \mathcal{F} = \frac{1}{2}\int_0^\infty d\nu \quad \int_1^{-1} d\mu \quad \mu\ \mathbf{I}(r, t; \vec{n}, \nu) \tag{10}$$

  and

$$\mathcal{P} = \frac{1}{2}\int_0^\infty d\nu \quad \int_1^{-1} d\mu \quad \mu^2\mathbf{I}(r, t; \vec{n}, \nu) \quad . \tag{11}$$

  Physically, ρ_R , $\mathcal{F}$ and $\mathcal{P}$, represent the radiation contribution to the: energy density, energy flux density and radial pressure, respectively.

From the above assumptions the energy momentum tensor can be written as $\hat{T}_{\mu\nu} = \hat{T}^M_{\mu\nu} + \hat{T}^R_{\mu\nu}$ where the material part is $\hat{T}^M_{\mu\nu}$ and the corresponding term for the radiation field, $\hat{T}^R_{\mu\nu}$, can be written as (Lindquist 1966; Mihalas & Mihalas 1984):

$$\hat{T}^R_{\mu\nu} = \begin{pmatrix} \rho_R & -\mathcal{F} & 0 & 0 \\ -\mathcal{F} & \mathcal{P} & 0 & 0 \\ 0 & 0 & \frac{1}{2}(\rho_R - \mathcal{P}) & 0 \\ 0 & 0 & 0 & \frac{1}{2}(\rho_R - \mathcal{P}) \end{pmatrix} . \tag{12}$$

Notice the induced anisotropy in the $\hat{T}^R_{\mu\nu}$ due to the radiation field.

Then, the energy-momentum tensor in the local co-moving frame takes the following form:

$$\hat{T}_{\mu\nu} = \left[(\rho + \rho_R) + P + \frac{1}{2}\,(\rho_R - \mathcal{P})\right]\hat{U}_\mu\hat{U}_\nu - \left(P + \frac{1}{2}\,(\rho_R - \mathcal{P})\right)\eta_{\mu\nu}$$

$$+ \frac{1}{2}(3\mathcal{P} - \rho_R)\hat{\chi}_\mu\hat{\chi}_\nu + \hat{F}_\mu\hat{U}_\nu + \hat{F}_\nu\hat{U}_\mu\ ; \tag{13}$$

where $\eta_{\mu\nu} = diag\,(1,-1,-1,-1)\,, \hat{U}_\mu = (1,0,0,0)$, $\hat{\chi}_\mu = (0,1,0,0)$ and $\hat{F}_\mu = (0,-\mathcal{F},0,0)$.

Now following Herrera et al (1994), in order to find the energy momentum tensor as seen by this observer co-moving with the fluid, we should perform an infinitesimal rotation around the symmetry axis, i.e.

$$\bar{T}_{\mu\nu} = \begin{pmatrix} \rho+\rho_R & -\mathcal{F} & 0 & \frac{1}{2}\mathcal{D}\,(3\rho_R-\mathcal{P}) \\ -\mathcal{F} & P+\mathcal{P} & 0 & -\mathcal{D}\mathcal{F} \\ 0 & 0 & P+\frac{1}{2}\,(\rho_R-\mathcal{P}) & 0 \\ \frac{1}{2}\mathcal{D}\,(3\rho_R-\mathcal{P}) & -\mathcal{D}\mathcal{F} & 0 & P+\frac{1}{2}\,(\rho_R-\mathcal{P}) \end{pmatrix}, \tag{14}$$

where $\mathcal{D}\,(u,r,\theta)$ is associated with the local "dragging of inertial frames" effect, which in the slow rotation limit $\mathcal{D}$ will also be taken up to first order.

Once minkowskian co-moving energy momentum tensor is built in terms of physical observables on a local frame (ρ, P, ρ_R , $\mathcal{F}$, $\mathcal{P}$,and $\mathcal{D}$), it can be transformed from the local minkowskian co-moving coordinates (t,x,y,z) to the curvilinear not co-moving Bondi coordinates (u,r,θ,ϕ) as

$$T_{\alpha\beta} = \frac{\partial\hat{x}^\gamma}{\partial x^\alpha}\,\frac{\partial\hat{x}^\lambda}{\partial x^\beta}\,L^\mu_\gamma(\vec{\omega})\,L^\nu_\lambda(\vec{\omega})\,\bar{T}_{\mu\nu}\,; \tag{15}$$

where $L^\nu_\lambda(\vec{\omega})$ is a Lorentz boost, written as

$$L^\mu_\gamma(\vec{\omega}) = \begin{pmatrix} \gamma & -\gamma\omega_x & 0 & -\gamma\omega_z \\ -\gamma\omega_x & 1+\frac{\omega_x^2(\gamma-1)}{\omega^2} & 0 & \frac{\omega_x\omega_z(\gamma-1)}{\omega^2} \\ 0 & 0 & 1 & 0 \\ -\gamma\omega_z & \frac{\omega_x\omega_z(\gamma-1)}{\omega^2} & 0 & 1+\frac{\omega_z^2(\gamma-1)}{\omega^2} \end{pmatrix}, \tag{16}$$

with

$$\gamma = \frac{1}{\sqrt{1-\omega^2}} \qquad \text{and} \qquad \omega^2 = \omega_x^2+\omega_z^2. \tag{17}$$

Observe that $\partial\hat{x}^\gamma/\partial x^\alpha$ are coordinate transformations connecting (t,x,y,z) with (u,r,θ,ϕ) which can be identify from equations (3) through (5).

In radiation coordinates the radial and orbital velocities of matter are given by

$$\frac{\mathrm{d}r}{\mathrm{d}u} = \frac{V}{r} : \frac{\omega_x}{1-\omega_x} \quad \text{and} \quad \frac{\mathrm{d}\phi}{\mathrm{d}u} = \frac{\omega_z}{1-\omega_x}\frac{1}{r\sin(\theta)}e^\beta\sqrt{\frac{V}{r}}, \tag{18}$$

respectively.

Now, using the metric (2), the energy momentum tensor (14), the transformation (15) and considering the slow rotation limit (i.e. first order in the orbital velocity ω_z, Kerr parameter $\tilde{\alpha}$ and the dragging function $\mathcal{D}$), we can write the Einstein equations as

- $8\pi T_{uu} = G_{uu}$:

$$\left(1-\frac{2\widetilde{m}}{r}\right)\frac{8\pi r^2}{\omega_x^2-1}\left[\rho+\rho_R-\mathcal{F}+(2\omega_x+1)\,\mathcal{F}+\omega_x^2\,(P+\mathcal{P})\right] \tag{19}$$

$$= \quad 2\left(1-\frac{2\widetilde{m}}{r}\right)\widetilde{m}_1-\frac{\widetilde{m}_{22}}{r}-\frac{\widetilde{m}_2}{r}\cot\theta-2e^{-2\beta}\widetilde{m}_0+3\left(1-\frac{2\widetilde{m}}{r}\right)\beta_2-\frac{6\widetilde{m}_2}{r}\beta_2 \ ,$$

- $8\pi T_{ur} = G_{ur}$:

$$\frac{8\pi r^2}{1+\omega_x}\left[\rho+\rho_R-\mathcal{F}-\omega_x\,(P+\mathcal{P}-\mathcal{F})\right]=2\widetilde{m}_1-\beta_{22}-\beta_2\cot(\theta)-\beta_2^2 \ , \tag{20}$$

- $8\pi T_{rr} = G_{rr}$:

$$2\pi r\left(1-\frac{2\widetilde{m}}{r}\right)^{-1}\left(\frac{1-\omega_x}{1+\omega_x}\right)\left[\rho+P+\rho_R+\mathcal{P}-2\mathcal{F}\right]=\beta_1 \ , \tag{21}$$

- $8\pi T_{\theta\theta} = G_{\theta\theta}$:

$$4\pi r^2\left[2P-\mathcal{P}+\rho_R\right]= \quad 2\beta_2\cot\theta-\widetilde{m}_{11}r-2e^{-2\beta}r^2\beta_{01}-6\beta_1\widetilde{m}_1 r$$

$$+3\beta_1 r+\beta_2^2+\left(1-\frac{2\widetilde{m}}{r}\right)\left(4\beta_1^2 r+2\beta_{11}r-\beta_1\right)r \ , \tag{22}$$

- $8\pi T_{u\theta} = G_{u\theta}$:

$$0=\left(1-\frac{2\widetilde{m}}{r}\right)(r\beta_{21}+4r\beta_1\beta_2-\beta_2)-\widetilde{m}_{21}-2\beta_2\widetilde{m}_1+\frac{\widetilde{m}_2}{r}-e^{-2\beta}r\beta_{02}-4\beta_1\widetilde{m}_2 \ , \tag{23}$$

- $8\pi T_{r\theta} = G_{r\theta}$:

$$0=\beta_{21}-\frac{2}{r}\beta_2 \ , \tag{24}$$

- $8\pi T_{\theta\phi} = G_{\theta\phi}$:

$$0=\left(1-\frac{2\widetilde{m}}{r}\right)r^2\,(4\beta_2\beta_1-\beta_{21})+\widetilde{m}_2\,(1-4\beta_1 r)-r\widetilde{m}_{21}$$

$$-2\beta_2\left(\widetilde{m}_1 r-\widetilde{m}\right)-e^{-2\beta}r^2\,(\beta_{21}-\beta_{02})-2\beta_2 e^{-2\beta}r^2\,(\beta_1-\beta_0) \ , \tag{25}$$

- $8\pi T_{r\phi}=G_{r\phi}$:

$$
\begin{aligned}
&8\pi r\left\{-\frac{r}{2\sin\theta}\left(\frac{1-\omega_x}{1+\omega_x}\right)^{\frac{1}{2}}\left(1-\frac{2\widetilde{m}}{r}\right)^{-\frac{1}{2}}\left(2\mathcal{F}+\mathcal{P}-3\rho_R\right)\mathcal{D}\right.\\
&-\widetilde{\alpha}\left(1-\frac{2\widetilde{m}}{r}\right)^{-1}\left(\frac{\omega_x-1}{\omega_x+1}\right)\left(\rho+P+\rho_R+\mathcal{P}-2\mathcal{F}\right)-\widetilde{\alpha}\frac{e^{2\beta}}{\omega_x+1}\left[\rho+\rho_R-\mathcal{F}-\omega_x\left(P+\mathcal{P}-\mathcal{F}\right)\right]\\
&+\frac{r}{2\sin\theta}\left(1-\frac{2\widetilde{m}}{r}\right)^{-\frac{1}{2}}\frac{\omega_z}{\omega_x\left(\omega_x+1\right)}\left[-2\omega_x\left(P+\mathcal{P}+\mathcal{F}\left(\frac{1}{f}-1\right)\right)+\right. \qquad (26)\\
&\left.\left.\left(3\mathcal{P}-\rho_R-2\mathcal{F}\right)\left(\omega_x+1-\sqrt{1-\omega_x^2}\right)\right]\right\}\\
&= \quad \widetilde{\alpha}\left[2r\left(\beta_1+\beta_0\right)-1+r^2\left(\beta_{11}-\beta_{01}\right)+e^{2\beta}\left(1-2\widetilde{m}_1\right)+e^{2\beta}\beta_2\left(\beta_2-3\cot\theta\right)+e^{2\beta}\beta_{22}\right] ,
\end{aligned}
$$

- $8\pi T_{u\phi}=G_{u\phi}$:

$$
\begin{aligned}
&8\pi r^2\left\{\frac{r}{2\sin\theta\sqrt{1-\omega_x^2}}\left(1-\frac{2\widetilde{m}}{r}\right)^{\frac{1}{2}}\left(2\omega_x\mathcal{F}-\mathcal{P}+3\rho_R\right)\mathcal{D}+\right.\\
&\frac{\widetilde{\alpha}}{\omega_x+1}\left[2\left(\rho+\rho_R-\mathcal{F}\right)-\omega_x\left(P+\mathcal{P}-\mathcal{F}\right)\right]+\frac{\widetilde{\alpha}e^{2\beta}}{\omega_x^2-1}\left(1-\frac{2\widetilde{m}}{r}\right)\left[\rho+\rho_R-\mathcal{F}+\left(\omega_x+1\right)^2\mathcal{F}\right.\\
&\left.+\omega_x^2\left(P+\mathcal{P}-\mathcal{F}\right)\right]+\frac{r\omega_z}{2\omega_x\sin\theta\left(1-\omega_x^2\right)}\left[2\omega_x\left(\rho+P+\rho_R+\mathcal{P}-2\mathcal{F}\right)+2\mathcal{F}\left(\omega_x+1\right)^2\right.\\
&\left.\left.+\sqrt{1-\omega_x^2}\left[2\mathcal{F}+\omega_x\left(3\mathcal{P}-\rho_R\right)\right]\right]\right\}\\
&= \quad \widetilde{\alpha}\left\{\left(1-\frac{2\widetilde{m}}{r}\right)\left[r^2\left(4\beta_0\beta_1-4\beta_1^2+\beta_{01}\right)-\left(\beta_0-3\beta_1\right)r-1\right]\right. \qquad (27)\\
&\quad +r\left[\left(\beta_0-3\beta_1\right)\left(1-2\widetilde{m}_1\right)-\widetilde{m}_{01}+\widetilde{m}_{11}-\frac{\widetilde{m}_0}{r}\left(4\beta_1r-3\right)\right]+e^{2\beta}\left(1-\frac{2\widetilde{m}}{r}\right)\left(1-2\widetilde{m}_1\right)\\
&\quad +e^{-2\beta}r^2\left(\beta_{01}-\beta_{00}\right)-e^{2\beta}\left(1-\frac{2\widetilde{m}}{r}\right)\left(3\beta_2^2+6\beta_2\cot\theta+e^{-2\beta}\beta_{11}r^2\right)\\
&\quad \left.+\frac{e^{2\beta}}{r}\left(\widetilde{m}_{22}+6\beta_2\widetilde{m}_2+3\widetilde{m}_2\right)-\beta_2\left(\beta_2-3\cot\theta\right)-\beta_{22}\right\} .
\end{aligned}
$$

Differentiation with respect to u, r and θ are denoted by subscripts 0,1 and 2, respectively. As in reference Herrera et al (1994) only six of the eight physical variables (ω_x, ω_z, ρ, P, ρ_R, $\mathcal{F}$, $\mathcal{P}$ and $\mathcal{D}$), can be algebraically obtained, in terms of the metric functions $\beta\left(u,r,\theta\right)$ and $\tilde{m}\left(u,r,\theta\right)$ and their derivatives, from field equations (19) through (27) . Therefore, more information (equations) has to be provided to this system in order to solve the physical variables. The idea will be to supply relations among the radiation physical variables ρ_R, $\mathcal{F}$, and $\mathcal{P}$. Next section will be devoted to describe these essential relations.

3. Closures relations and the limits for the radiation field

In order to deal with more realistic scenarios, the microphysical framework of the interrelation between matter and radiation have to be considered. The relativistic Boltzmann Transport Equation must be coupled to the hydrodynamic equations in order to obtain the evolution of the system as well as the spectrum and angular distribution of the radiation field (Lindquist 1966) Neglecting effects as polarization, dispersion and coherence, a covariant special relativistic equation of radiation transport has been proposed as (Anderson & Spiegel 1972; Ali & Romano 1994):

$$(u^\mu + l^\mu)\left\{\nabla_\mu\ \mathbf{I} + 4\mathbf{I}\ l^\sigma\ \nabla_\mu\ u_\sigma + l^\rho\ l^\sigma\ \frac{\partial\ \mathbf{I}}{\partial\ l^\rho}\ \nabla_\mu\ u_\sigma + u^\rho\ l^\sigma \frac{\partial\ \mathbf{I}}{\partial\ l^\rho}\ \nabla_\mu\ u_\sigma - \frac{\partial\ \mathbf{I}}{\partial\ l^\rho}\ \nabla_\mu\ u^\rho\right\} = \rho(\epsilon_0 - \kappa I)\ , \tag{28}$$

where $l_\mu l^\mu = 1$ with $l_\mu u^\mu = 0$; the four velocity of the fluid is u^μ; ρ is proper density of the medium; the quantities ϵ_0 and κ are the emissivity and the absorption coefficient, respectively. This transfer equation has several important difficulties. The most important are: the lack of information about the coupling between radiation and ultradense matter and its mathematical complexity, although some understanding is emerging recently(Efimov et al 1997; Wehrse & Baschek 1999).

One of the possible strategies to circumvent the difficulty of solving the radiation transfer equation is to consider one of the two physical reasonable limits for the radiation field which describe a significant variety of astrophysical scenarios(Mihalas & Mihalas 1984). The *free streaming out* limit assumes that radiation (neutrinos and/or photons) mean free path is of the order of the dimension of the sphere. This was the case considered in Herrera et al (1994) and it can be expressed as

$$\rho_R = \mathcal{F} = \mathcal{P} = \hat{\epsilon}\ . \tag{29}$$

The other limit for the radiation field is the *diffusion limit approximation,* where radiation is considered to flow with a mean free path much smaller than the characteristic length of the system. Within this limit, radiation is locally isotropic and we have

$$\rho_R = 3\mathcal{P} \quad \text{and} \quad \mathcal{F} = \hat{q}\ . \tag{30}$$

In order to simulate more realistically the matter and radiation interaction, it seems more reasonable to have a parameter which varies between the above mentioned limits. This is the idea of the flux and the variable Eddington factor an they can be summarized as follows. From equations (10) through (11) it is convenient to define the following normalized quantities

$$\varphi(\vec{r},t,\Omega) = \frac{I(\vec{r},t,\Omega)}{\rho_R}, \quad \tilde{\mathbf{f}} = \int_{4\pi} \varphi(\vec{r},t,\Omega)\vec{n}d\Omega \quad \text{and} \quad \mathbb{K} = \int_{4\pi} \varphi(\vec{r},t,\Omega)\vec{n}\otimes\vec{n}d\Omega, \tag{31}$$

The Eddington factor is, defined as the eigenvalue of the Pressure Tensor corresponding to the eigenvector $\vec{n}$ (unitary vector in the direction of the energy flux), i.e. $K^i_j n^j = \chi n^i$ (Anile et al 1991). Thus,

$$\tilde{\mathbf{f}} \Rightarrow f^i = f n^i \quad \text{and} \quad \mathbb{K} \Rightarrow K^{ij} = \frac{1}{2}\left\{(1-\chi)\delta^{ij} + (3\chi - 1)n^i n^j\right\}\ . \tag{32}$$

In the one-dimensional case the above equations lead to

$$f = \frac{\mathcal{F}}{\rho_R} \quad \text{and} \quad \chi = \frac{\mathcal{P}}{\rho_R} \, . \tag{33}$$

Which are called the flux and the variable Eddington factor, respectively.

In order to "close" this problem and to algebraically obtain six of the above mentioned physical variables, namely ω_x, ω_z, ρ, P, $\mathcal{F}$, and $\mathcal{D}$, from field equations (19) through (27) and the radiation parameter (33) (or in general (31)) we need to state a relation between f, and χ. It is easy to perceive that such a relation could exist. In fact, it is noticeable that in the corresponding limits for the radiation field, i.e. *diffusion limit approximation* and *free streaming out* we have

$$\left.\begin{array}{l} \mathcal{P} = \frac{1}{3}\rho_R \Rightarrow f \longrightarrow 0 \quad \text{and} \quad \chi = \frac{1}{3} \\ \\ \mathcal{F} = \mathcal{P} = \rho_R \Rightarrow f = 1 \quad \text{and} \quad \chi = 1 \end{array}\right\} \Rightarrow 0 \leq f \leq 1 \quad \text{and} \quad \frac{1}{3} \leq \chi(f) \leq 1 \tag{34}$$

Causality requirement implies the following supplementary conditions on f and χ, in order to define a physically plausible region in the $\{f, \chi, \mathrm{d}\chi/\mathrm{d}f\}$ space (Pons et al 2000)

$$\|f\| \leq 1, \quad f^2 \leq \chi \leq 1 \quad \text{and} \quad -\frac{1-\chi}{1+f} \leq \frac{\mathrm{d}\chi}{\mathrm{d}f} \leq \frac{1-\chi}{1-f} \tag{35}$$

There are several of those closure relations reported in the literature (see two recent comprehensive discussions on this subject in Pons et al (2000) and Smit et al (2000) and references therein). Few of them are simply *ad hoc* relations that smoothly interpolate the radiation field between the diffusive and free-streaming regimes. Others, are derived from a maximum entropy principle or from a given, or assumed, angular dependence of the radiative distribution functions. Even one of them has been motivated from direct transport calculations. Six of the most frequent found closure relations are listed in Table 1. In this list the first four could be considered as "analytical" closure relations, while the last two are referred as numerical, because for a given flux factor f, the nonlinear equation $f = \coth\beta - (1/\beta)$ has to be numerically solved in order to obtain the variable Eddington factor χ.

In the present paper we are going to explore some of the effects of dissipation on the evolution of slowing rotating radiating matter configuration in General Relativity. We shall evaluate how independent are these effects from an explicit closure relation and/or a specific EoS chosen. Particularly, some results concerning the influence of the junction conditions on the eccentricity and the radiation scheme evaluated at the surface, will be presented in the next section. The strategy we follow to close the system of Einstein field equations with a radiation field, contrasts with the standard iterative method for solving the moment equations (10), and (11), starting from an estimated Eddington factor (see Mihalas & Mihalas (1984) and Rampp & Janka (2002) and references therein).

Thus, by using equations (33), the Einstein field equations (19)-(27) can be re-written as:

- $8\pi T_{uu} = G_{uu}$:

$$\left(1-\frac{2\widetilde{m}}{r}\right)\frac{8\pi r^2}{\omega_x^2-1}\left[\rho+\omega_x^2 P+\left(\frac{1}{f}+2\omega_x+\omega_x^2\frac{\chi}{f}\right)\mathcal{F}\right]$$

$$=2\left(1-\frac{2\widetilde{m}}{r}\right)\widetilde{m}_1-\frac{\widetilde{m}_{22}}{r}-\frac{\widetilde{m}_2}{r}\cot\theta-2e^{-2\beta}\widetilde{m}_0+3\left(1-\frac{2\widetilde{m}}{r}\right)\beta_2-\frac{6\widetilde{m}_2}{r}\beta_2\ , \tag{36}$$

- $8\pi T_{ur} = G_{ur}$:

$$\frac{8\pi r^2}{1+\omega_x}\left[\rho-\omega_x P+\left(\frac{1}{f}-1+\omega_x\left(1-\frac{\chi}{f}\right)\right)\mathcal{F}\right]=2\widetilde{m}_1-\beta_{22}-\beta_2\cot(\theta)-\beta_2^2\ , \tag{37}$$

- $8\pi T_{rr} = G_{rr}$:

$$2\pi r\left(1-\frac{2\widetilde{m}}{r}\right)^{-1}\left(\frac{1-\omega_x}{1+\omega_x}\right)\left[\rho+P+\left(\frac{1}{f}+\frac{\chi}{f}-2\right)\mathcal{F}\right]=\beta_1\ , \tag{38}$$

- $8\pi T_{\theta\theta} = G_{\theta\theta}$:

$$4\pi r^2\left[2P+\frac{1}{f}(1-\chi)\mathcal{F}\right]=2\beta_2\cot\theta-\widetilde{m}_{11}r-2e^{-2\beta}r^2\beta_{01}-6\beta_1\widetilde{m}_1 r$$

$$+3\beta_1 r+\beta_2^2+\left(1-\frac{2\widetilde{m}}{r}\right)\left(4\beta_1^2 r+2\beta_{11}r-\beta_1\right)r\ , \tag{39}$$

- $8\pi T_{u\theta} = G_{u\theta}$:

$$0=\left(1-\frac{2\widetilde{m}}{r}\right)(r\beta_{21}+4r\beta_1\beta_2-\beta_2)-\widetilde{m}_{21}-2\beta_2\widetilde{m}_1+\frac{\widetilde{m}_2}{r}-e^{-2\beta}r\beta_{02}-4\beta_1\widetilde{m}_2\ , \tag{40}$$

- $8\pi T_{r\theta} = G_{r\theta}$:

$$0=\beta_{21}-\frac{2}{r}\beta_2\ , \tag{41}$$

- $8\pi T_{\theta\phi} = G_{\theta\phi}$:

$$0=\left(1-\frac{2\widetilde{m}}{r}\right)r^2(4\beta_2\beta_1-\beta_{21})+\widetilde{m}_2(1-4\beta_1 r)-r\widetilde{m}_{21}$$

$$-2\beta_2\left(\widetilde{m}_1 r-\widetilde{m}\right)-e^{-2\beta}r^2(\beta_{21}-\beta_{02})-2\beta_2 e^{-2\beta}r^2(\beta_1-\beta_0)\ , \tag{42}$$

- $8\pi T_{r\phi} = G_{r\phi}$:

$$
\begin{aligned}
8\pi r \Bigg\{ & -\frac{r}{2\sin\theta}\left(\frac{1-\omega_x}{1+\omega_x}\right)^{\frac{1}{2}}\left(1-\frac{2\widetilde{m}}{r}\right)^{-\frac{1}{2}}\left(2+\frac{\chi}{f}-\frac{3}{f}\right)\mathcal{F}\mathcal{D} \\
& -\widetilde{\alpha}\left(1-\frac{2\widetilde{m}}{r}\right)^{-1}\left(\frac{\omega_x-1}{\omega_x+1}\right)\left(\left(\frac{1}{f}+\frac{\chi}{f}-2\right)\mathcal{F}+\rho+P\right) \\
& -\widetilde{\alpha}\frac{e^{2\beta}}{\omega_x+1}\left[\left(\frac{1}{f}-1-\omega_x\left(\frac{\chi}{f}-1\right)\right)\mathcal{F}+\rho-\omega_x P\right] \qquad (43) \\
& +\frac{r}{2\sin\theta}\left(1-\frac{2\widetilde{m}}{r}\right)^{-\frac{1}{2}}\frac{\omega_z}{\omega_x\left(\omega_x+1\right)}\left[P+\left(\omega_x\left(\chi-3\right)+3\chi+\left(3\chi-1-2f\right)\sqrt{\left(1-\omega_x^2\right)}\right)\frac{\mathcal{F}}{f}\right]\Bigg\} \\
= & \widetilde{\alpha}\left[2r\left(\beta_1+\beta_0\right)-1+r^2\left(\beta_{11}-\beta_{01}\right)+e^{2\beta}\left(1-2\widetilde{m}_1\right)+e^{2\beta}\beta_2\left(\beta_2-3\cot\theta\right)+e^{2\beta}\beta_{22}\right] ,
\end{aligned}
$$

- $8\pi T_{u\phi} = G_{u\phi}$:

$$
\begin{aligned}
8\pi r^2 \Bigg\{ & \frac{r}{2\sin\theta\sqrt{1-\omega_x^2}}\left(1-\frac{2\widetilde{m}}{r}\right)^{\frac{1}{2}}\left(2\omega_x-\frac{\chi}{f}+\frac{3}{f}\right)\mathcal{F}\mathcal{D}+ \\
& +\frac{\widetilde{\alpha}}{\omega_x+1}\left[2\rho-\omega_x P+\left(\frac{2}{f}-2-\omega_x\left(\frac{\chi}{f}-1\right)\right)\mathcal{F}\right]+\frac{\widetilde{\alpha}e^{2\beta}}{\omega_x^2-1}\left(1-\frac{2\widetilde{m}}{r}\right)\left[\frac{\rho f+\omega_x^2 P f}{f}+\right. \\
& \left.+\frac{1+2\omega_x f+\omega_x^2\chi}{f}\mathcal{F}\right]+\frac{r\omega_z}{\omega_x\sin\theta\left(1-\omega_x^2\right)}\left[\frac{\omega_x+\omega_x\chi+f\omega_x^2+f}{f}\mathcal{F}+\frac{\omega_x\rho f+\omega_x P f}{f}\right. \\
& \left.+\sqrt{1-\omega_x^2}\left(1+\frac{\omega_x}{2}\left(3\frac{\chi}{f}-\frac{1}{f}\right)\right)\mathcal{F}\right]\Bigg\} \\
= & \widetilde{\alpha}\Bigg\{\left(1-\frac{2\widetilde{m}}{r}\right)\left[r^2\left(4\beta_0\beta_1-4\beta_1^2+\beta_{01}\right)-\left(\beta_0-3\beta_1\right)r-1\right]+ \qquad (44) \\
& +r\left[\left(\beta_0-3\beta_1\right)\left(1-2\widetilde{m}_1\right)-\widetilde{m}_{01}+\widetilde{m}_{11}-\frac{\widetilde{m}_0}{r}\left(4\beta_1 r-3\right)\right]+e^{2\beta}\left(1-\frac{2\widetilde{m}}{r}\right)\left(1-2\widetilde{m}_1\right)+ \\
& +e^{-2\beta}r^2\left(\beta_{01}-\beta_{00}\right)-e^{2\beta}\left(1-\frac{2\widetilde{m}}{r}\right)\left(3\beta_2^2+6\beta_2\cot\theta+e^{-2\beta}\beta_{11}r^2\right)+ \\
& +\frac{e^{2\beta}}{r}\left(\widetilde{m}_{22}+6\beta_2\widetilde{m}_2+3\widetilde{m}_2\right)-\beta_2\left(\beta_2-3\cot\theta\right)-\beta_{22}\Bigg\} .
\end{aligned}
$$

In principle, for all cases listed in Table 1 (including the numerical closures relations) it is possible to algebraically obtain the remaining six physical variables, ω_x, ω_z, ρ, P, $\mathcal{F}$, and $\mathcal{D}$, from the system (36) through (44), in terms of the Kerr parameter, $\widetilde{\alpha}$, the flux factor, f , the metric functions $\beta\left(u,r,\theta\right)$, $\tilde{m}\left(u,r,\theta\right)$ and their derivatives.

4. Eddington factor, flux factor and junction conditions

In this section, following Herrera et al (1994) we should match the interior fluid spheroid to the exterior Kerr-Vaidya solution (equation (1)). Therefore, the continuity of the *first* and the *second fundamental* (g_{ij} and K_{ij}) forms across the matching surface are needed. These requirements are equivalent to demand the continuity of the *tetrad components* and *spin coefficient* of the metrics (1) and (2) across the boundary surface $r = a\,(u)$ (Herrera & Jiménez 1983).

4.1. Junction conditions for a slowly rotating configuration

The Newman-Penrose null tetrad components for the metrics (1) and (2) (see reference Herrera et al (1994) to find the expressions of the spin coefficients for these two metrics) are:

- for the exterior metric

$$l^{\mu} = \delta^{\mu}_{r}; \qquad n^{\mu} = \delta^{\mu}_{u} - \frac{1}{2}\left[1 - \frac{2mr}{r^2 + \alpha^2\cos^2(\theta)}\right]\delta^{\mu}_{r} \tag{45}$$

$$\text{and} \qquad m^{\mu} = \frac{1}{\sqrt{2}\,(r + i\alpha\cos\theta)}\left[i\alpha\sin\theta\,(\delta^{\mu}_{u} - \delta^{\mu}_{r}) + \delta^{\mu}_{\theta} + i\csc\theta\delta^{\mu}_{\phi}\right]\ ; \tag{46}$$

- for the interior metric (2)

$$l^{\mu} = e^{-2\beta}\delta^{\mu}_{r}; \qquad n^{\mu} = \delta^{\mu}_{u} - \frac{1}{2}e^{-2\beta}\left[1 - \frac{2\tilde{m}r}{r^2 + \widetilde{\alpha}^2\cos^2(\theta)}\right]\delta^{\mu}_{r} \tag{47}$$

$$\text{and} \qquad m^{\mu} = \frac{1}{\sqrt{2}\,(r + i\widetilde{\alpha}\cos\theta)}\left[i\widetilde{\alpha}\sin\theta\,(\delta^{\mu}_{u} - \delta^{\mu}_{r}) + \delta^{\mu}_{\theta} + i\csc\theta\delta^{\mu}_{\phi}\right]. \tag{48}$$

The continuity of the tetrad components across the boundary surface $r = a(u)$ implies

$$\beta_a = 0; \qquad \tilde{m}_a = m \qquad \text{and} \qquad \widetilde{\alpha}_a = \alpha\ , \tag{49}$$

and the continuity of the spin coefficients τ, γ, and ν lead to

$$\beta_{1a}\left(1 - \frac{2m}{a}\right) - \beta_{0a} = \frac{\tilde{m}_{1a}}{2a}; \qquad \beta_{2a} = \tilde{m}_{2a} = 0 \qquad \text{and} \tag{50}$$

$$\alpha\,(\beta_{1a} - \beta_{0a}) = \alpha\,(m_{0a} - \tilde{m}_{0a} + \tilde{m}_{1a}) = 0, \tag{51}$$

which means that $(\beta_{1a} - \beta_{0a})$ and $(m_{0a} - \tilde{m}_{0a} + \tilde{m}_{1a})$ are of order α.

Now, evaluating the field equations (19) - (27) (or equivalently (36) through (44),) at $r = a(u)$ and considering the above results (49) through (51), we obtain that, on these coordinates and up

to the first order in α, the metric coefficients β and $\tilde{m}$ are *independent of the angular variable* and consequently the physical variables: ω_x, ρ, P, and $\mathcal{F}$ are also $\theta-$independent (see Herrera et al (1994) for details).

Next, expanding β near the surface, $\beta_{0a} + \dot{a}\beta_{1a} = 0$, in equation (50) and using that β is continuous and vanishes at the outside the matter configuration we obtain that

$$\beta_{1a}\left(1-\frac{2\,\tilde{m}}{a}\right)-\beta_{0a}=\frac{\tilde{m}_{1a}}{2a}\Longrightarrow \dot{a}=\left(1-\frac{2\tilde{m}_a}{a}\right)\left[\frac{(\rho_a+\rho_{Ra}-\mathcal{F}_a)\,\omega_{xa}-(P_a+\mathcal{P}_a-\mathcal{F}_a)}{(\rho_a+\rho_{Ra}+P_a+\mathcal{P}_a-2\mathcal{F}_a)\,(1-\omega_{xa})}\right]\,, \quad (52)$$

where $\dot{a} = \mathrm{d}r/\mathrm{d}u$. On the other hand, from equation (18) it follows that

$$\dot{a}=\left(1-\frac{2\tilde{m}_a}{a}\right)\frac{\omega_{xa}}{1-\omega_{xa}}. \quad (53)$$

Equating (52) and (53), it is obtained that the emerging energy flux density compensates the total pressure (hydrodynamic and radiation) inside the configuration (Aguirre et al 1994), i.e.

$$\mathcal{F}_a = P_a + \mathcal{P}_a\ . \quad (54)$$

Now, expanding β and $\tilde{m}$ near the surface in equation (51) we conclude that

$$\beta_{1a}\,(1+\dot{a})\approx\alpha\Longrightarrow\beta_{1a}\,(1+\dot{a})=v(u)\alpha \quad \text{and} \quad \tilde{m}_{1a}\,(1+\dot{a})\approx\alpha\Longrightarrow\tilde{m}_{1a}\,(1+\dot{a})=q(u)\alpha\ . \quad (55)$$

Where $v(u)$ and $q(u)$ are arbitrary functions of the time-like coordinate u with $|v(u)| \lessapprox 1$ and $|q(u)| \lessapprox 1$ in order to keep valid the approximation. Additionally, by using field equations (20) and (21), we get that

$$\begin{aligned}
&\beta_{1a}\,(1+\dot{a})\approx\alpha \quad\Longrightarrow\quad \frac{2\pi a\left(1-\omega_{xa}\dfrac{2\,\tilde{m}_a}{a}\right)}{\left(1-\dfrac{2\,\tilde{m}_a}{a}\right)(1+\omega_{xa})}\left[\rho_a+\rho_{Ra}-\mathcal{F}_a\right]\approx\alpha \\
&\qquad\text{and} \\
&\tilde{m}_{1a}\,(1+\dot{a})\approx\alpha \quad\Longrightarrow\quad \frac{a^2 4\pi}{1+\omega_{xa}^2}\left(1-\omega_{xa}\frac{2\,\tilde{m}_a}{a}\right)\left[\rho_a+\rho_{Ra}-\mathcal{F}_a\right]\approx\alpha\ ,
\end{aligned} \quad (56)$$

which impose restrictions on the physical variable evaluated at the surface of the distribution.

Also, it follows from the junction conditions (50) that

$$2a\beta_{1a}\left(1+\dot{a}-\frac{2\tilde{m}_a}{a}\right)=\tilde{m}_{1a} \quad\Longleftrightarrow\quad 2a\beta_{1a}\left(1-\frac{2\tilde{m}_a}{a}\right)=\tilde{m}_{1a}\,(1-\omega_{xa})\,. \quad (57)$$

Thus, we obtain an expression relating $v(u)$ and $q(u)$, namely

$$2a\left(1+\dot{a}-\frac{2\tilde{m}_a}{a}\right)v(u)=q(u) \qquad\Longleftrightarrow\qquad \frac{2a}{(1-\omega_{xa})}\left(1-\frac{2\tilde{m}_a}{a}\right)v(u)=q(u). \quad (58)$$

However, it can be checked by simple inspection that, because neither the field equations nor the junction conditions impose further limitations on these functions of u, one of them remains completely arbitrary for each model.

More over, at least for some models we have

$$\frac{2a}{(1-\omega_{xa})}\left(1-\frac{2\tilde{m}_a}{a}\right)\sim 1, \tag{59}$$

which becomes useful when selecting the order of magnitude of the initial parameters ($\tilde{m}_a, a$ and ω_{xa}) for the modelling of slowly rotating collapsing configurations (i.e. first order in the orbital velocity ω_z, Kerr parameter $\tilde{\alpha}$ and the dragging function $\mathcal{D}$), worked out in section 6.2.

The next section will be devoted to explore consequences of the radiation field, $T^R_{\mu\nu}$, in collapsing configurations in the slow rotation approximation.

4.2. The limits for the flux factor and the eccentricity

Now, from equations (33), and (54), we have

$$P_a=\mathcal{F}_a\left(1-\frac{\mathcal{P}_a}{\mathcal{F}_a}\right)\qquad\Longrightarrow P_a=\mathcal{F}_a\left(1-\frac{\chi_a}{f_a}\right). \tag{60}$$

If we assume that the hydrodynamic pressure and the outgoing energy flux have to be positive then we have that $(1-(\chi_a/f_a))\geq 0$. Figure 1 displays this factor for the different closure relations in Table 1. It is clear from this figure that the boundary conditions compel the impossibility to attain total diffusion regime (i.e. $f=0$) at the surface of the configuration. The roots of each curve representing a closure relation define the interval of acceptability for the values of the flux factor f . These intervals are displayed in the second column of Table 2. As it can be appreciated form Figure 1, only the *Levermore-Pomraning* closure relation does not meet this requirement. Up to the precision of our numerical calculation, the acceptable value for f that guarantees the positiveness of the hydrodynamic pressure is 1. Thus, considering the *Levermore-Pomraning* closure relation, junction conditions, up to the first order in Kerr rotation parameter, only allows free streaming out at the surface for this slowly rotating matter distribution. On the other hand, *Minerbo* closure relation seems to admits transport mechanism closer to the diffusion limit.

Because all these results emerge from the junction conditions that couple the internal and the external solutions, they are valid not only for axisymmetric configurations but also for spherical ones. It is also independent of the EoS and is present for all the closure relations we have listed in the Table 1.

Finally, expanding (7) for $\tilde{\alpha}\ll 1$, we get $\tilde{\alpha}$(Herrera et al 1998)

$$e=\frac{1}{r_s}\tilde{\alpha}-\frac{1}{2}\frac{1}{r_s^3}\tilde{\alpha}^3+\cdots\ , \tag{61}$$

as expected, up to first order, the eccentricity is proportional to $\tilde{\alpha}$. Now, using the field equation (20) evaluated at the surface $r = a\,(u)$, (55) and (58) we are lead to

$$\tilde{\alpha}_a = \alpha = \frac{2\pi a\left(\rho_a + \mathcal{F}_a\dfrac{(1-f_a)}{f_a}\right)\left(1-\omega_{xa}\dfrac{2\tilde{m}_a}{a}\right)}{(1+\omega_{xa})\left(1-\dfrac{2\tilde{m}_a}{a}\right)v(u)}, \tag{62}$$

and the surface eccentricity can be re-written as

$$e_a = \frac{2\pi\left[\rho_a + \mathcal{F}_a\dfrac{(1-f_a)}{f_a}\right]\left(1-\omega_{xa}\dfrac{2\tilde{m}_a}{a}\right)}{(1+\omega_{xa})\left(1-\dfrac{2\tilde{m}_a}{a}\right)v(u)}. \tag{63}$$

Notice that, $v(u)$ remains completely arbitrary and its choice completes the characterization of the model.

Because of the range of acceptability for the flux factor we also obtain a range for the eccentricity, i.e.

$$f_{\min\chi} \leq f \leq 1 \quad \Rightarrow \Lambda \leq e_{LE_a} \leq \Lambda\left(1+\frac{\mathcal{F}_a}{\rho_a}\frac{(1-f_a)}{f_a}\right) \quad \text{where} \quad \Lambda = \frac{2\pi\rho_a\left(1-\omega_{xa}\dfrac{2\tilde{m}_a}{a}\right)}{(1+\omega_{xa})\left(1-\dfrac{2\tilde{m}_a}{a}\right)v(u)} \tag{64}$$

Therefore, it is clear from Table 2 that radiation mechanism affects the oblateness of the configuration. This is to say, in these coordinates up to first order in $\tilde{\alpha}_a$ and for those models having $\Lambda > 0$, the eccentricity at the surface of a radiating configuration is greater for models near the diffusion limit approximation than for those in the free streaming out limit. Again, this result is also valid for any EoS with $0 \leqslant v(u) \leqslant 1$ and it is present for all the closure relations in the Table 1. For details of these calculations readers are referred to the following url link:
http://webdelprofesor.ula.ve/ciencias/nunez/CalculosIntermedios/EddintonFactor/clousuresTerenzio.html

In the next section we shall explore the effect of these closure relations on the collapse of a radiating, slow-rotating self-gravitating relativistic configuration.

5. The HJR method and Surface Equations

In order to obtain the evolution of the profiles of the physical variables, ω_x, ω_z, ρ, P, $\mathcal{F}$, and $\mathcal{D}$, we use an extension of the HJR method (Herrera et al 1980) to axially symmetric slowly rotating case (Herrera et al 1994).

First, we define two auxiliary variables which, in terms of the Eddington and the Flux factor,

can be written as

$$\widetilde{\rho} = \frac{\rho + \rho_R - \mathcal{F} - \omega_x(P + \mathcal{P} - \mathcal{F})}{1 + \omega_x} \equiv \frac{\rho - \omega_x P + \frac{1}{f}(1 - f - \omega_x(\chi - f))\mathcal{F}}{1 + \omega_x} \ , \tag{65}$$

and is called the effective density and, correspondingly, the effective pressure is

$$\widetilde{P} = \frac{P + \mathcal{P} - \mathcal{F} - \omega_x(\rho + \rho_R - \mathcal{F})}{1 + \omega_x} \equiv \frac{P - \omega_x \rho + \frac{1}{f}(\chi - f - \omega_x(1 - f))\mathcal{F}}{1 + \omega_x} \ . \tag{66}$$

With these *effective variables*, the metric elements (equations (20) and (21)) can be formally integrated as

$$\beta(u, r) = \int_a^r 2\pi\overline{r} \frac{\widetilde{\rho} + \widetilde{P}}{\left(1 - \frac{2\widetilde{m}}{\overline{r}}\right)} d\overline{r} \qquad \text{and} \qquad \widetilde{m}(u, r) = \int_0^r 4\pi \ \overline{r}^2 \ \widetilde{\rho} d\overline{r} \ . \tag{67}$$

Thus, if the r dependence of $\tilde{P}$ and $\tilde{\rho}$ are known, we can get the metric functions $\tilde{m}$ and β up to some functions of u related to the boundary conditions. This is one of the key points to transform the Einstein System into a system of (coupled nonlinear) ordinary differential equations on the time-like coordinate. Physically, the rationale behind the assumption on the r dependence of the *effective variables* $\tilde{P}$ and $\tilde{\rho}$, can be grasped in terms of the characteristic times for different processes involved in a collapse scenario. If the hydrostatic time scale $\mathcal{T}_{HYDR}$, which is of the order $\sim 1/\sqrt{G\rho}$ (where G is the gravitational constant and ρ denotes the mean density) is much smaller than the *Kelvin-Helmholtz* time scale ($\mathcal{T}_{KH}$), then in a first approximation the inertial terms in the equation of motion can be ignored (Kippenhahn & Weigert 1990). Therefore in this first approximation (quasi-stationary approximation) the r dependence of P and ρ are the same as in the static solution. Then the assumption that the *effective variables* (65) and (66) have the same r dependence as the physical variables of the static situation, represents a correction to that approximation, and is expected to yield good results whenever $\mathcal{T}_{KH} \gg \mathcal{T}_{HYDR}$. Fortunately enough, $\mathcal{T}_{KH} \gg \mathcal{T}_{HYDR}$, for almost all kind of stellar objects. Recently this rationale becomes intelligible and finds full justification within the context of a suitable definition of the post-quasi-static approximation for the gravitational collapse(Barreto et al 2002; Herrera et al 2002).

Those functions of the time-like coordinate u that remain arbitrary can be obtained from a system of ordinary differential equations (*The System of Surface Equations, SSE*) emerging from the junction conditions and both the field equations and some kinematic definitions evaluated at the boundary surface. The first surface equation is (53):

$$\dot{A} = F(\Omega - 1) \ . \tag{68}$$

Where we have scaled the radius a, the total mass $\tilde{m}_a = m$ and the timelike coordinate u by the total initial mass, $m(u = 0) = m(0)$, i.e.

$$A = \frac{a}{m(0)}, \qquad M = \frac{m}{m(0)}, \qquad u = \frac{u}{m(0)} \tag{69}$$

and we have also defined

$$F = 1 - \frac{2M}{A}, \qquad \text{and} \qquad \Omega = \frac{1}{1-\omega_{xa}} \, . \tag{70}$$

Again, the dot over the variable represents the derivative with respect to the time-like coordinate. The second *Surface Equation* emerges from the evaluation of equation (36) at $r = a_{+0}$. It takes the form of

$$\dot{M} = -FL \, , \tag{71}$$

where L representing the total luminosity can be written as

$$L = 4\pi A^2 \mathcal{F}_a \left(2\Omega - 1\right). \tag{72}$$

Now, using above equation (68) and definitions (69) and (70); we can re-state equation (71) as

$$\frac{\dot{F}}{F} = \frac{2L + (1-F)(\Omega - 1)}{A} \, . \tag{73}$$

Finally, after some straightforward manipulations, starting from field equations (37), (38) and (39), it is obtained

$$e^{2\beta}\left(\frac{\tilde{\rho}+\tilde{P}}{1-\frac{2\tilde{m}}{r}}\right)_{,0} - \frac{\partial \tilde{P}}{\partial r} - \frac{\tilde{\rho}+\tilde{P}}{1-\frac{2\tilde{m}}{r}}\left(4\pi r\tilde{P} + \frac{\tilde{m}}{r^2}\right) = \frac{-2}{r}\left(P + \frac{1}{2}\left(\rho_R - \mathcal{P}\right) - \tilde{P}\right), \tag{74}$$

which is the generalization of Tolman-Oppenheimer-Volkov (TOV) equation for any dynamic radiative situation. The third *Surface Equation* can be obtained evaluating (74) at $r = a_{+0}$, and it takes the form of:

$$\begin{aligned} 0 = \frac{\dot{\Omega}}{\Omega} + \frac{\dot{F}}{F} + \frac{(\tilde{\rho}_a)_{,0}}{\tilde{\rho}_a} + \frac{F\Omega^2\tilde{R}}{\tilde{\rho}_a} - \frac{2F\Omega}{A\tilde{\rho}_a}\left(P_a + \frac{\chi(f)\,\mathcal{F}_a}{2f}(\chi(f) - 1)\right) \\ + (\Omega - 1), \left(\frac{F\Omega\tilde{\rho}_{1a}}{\tilde{\rho}_a} - \frac{4\pi A(1-3\Omega)\tilde{\rho}_a}{\Omega} - \frac{3+F}{2A}\right), \end{aligned} \tag{75}$$

where

$$\tilde{R} = \left[\frac{\partial \tilde{P}}{\partial r} + \frac{\tilde{\rho}+\tilde{P}}{1-\frac{2\tilde{m}}{r}}\left(4\pi r\tilde{P} + \frac{\tilde{m}}{r^2}\right)\right]_a \, . \tag{76}$$

Equations (68), (73) and (75) conform the *SSE* which coincides with the spherically symmetric case (Aguirre et al 1994) because that up to the first order in $\tilde{\alpha}$, the metric functions $\tilde{m}$ and β are found to be independent on the angular variables. This system may be integrated numerically for any given radial dependence of the *effective variables,* providing the total luminosity, a closure relation and a flux factor f. The remaining two equations (43) and (44) provide a simple θ-dependence on the physical variables ω_z, and $\mathcal{D}$, i.e.

$$\omega_z = \tilde{\alpha}\sin\theta \; \mathcal{Y}\left[\tilde{m}, \beta; \text{their derivatives}; r\right] \quad \text{and} \quad \mathcal{D} = \tilde{\alpha}\sin\theta \; \mathcal{Z}\left[\tilde{m}, \beta; \text{ their derivatives; } r\right] \tag{77}$$

The restriction due to the junctions conditions for slowly rotating spheroids (56) can be re-written in terms of the effective variables as

$$2\pi A\frac{\widetilde{\rho}_a+\widetilde{P}_a}{F}\left(1+\dot{A}\right)=\tilde{v}\,(u)\,\alpha\quad\text{and}\quad 4\pi\ A^2\ \widetilde{\rho}_a\left(1+\dot{A}\right)=\tilde{q}\,(u)\,\alpha, \tag{78}$$

and equation, at least for some models, (59) can be re-phrased in a very compact form:

$$2AF\Omega\sim 1 \tag{79}$$

Again, this equation becomes very useful when selecting a set of initial conditions to integrate the *SSE.*

For completeness, we outline here a brief *resumé* of the HJR method for isotropic slowly rotating radiating fluid spheres (see Herrera et al (1994), for details):

1. Take a static interior solution of the Einstein Equations for a fluid with spherical symmetry, $\rho_{static}=\rho(r)$ and $P_{static}=P(r)$.

2. Assume that the r dependence of $\tilde{P}$ and $\tilde{\rho}$ are the same as that of P_{static} and ρ_{static}, respectively. Be aware of the boundary condition:

$$\tilde{P}_a=-\omega_{xa}\tilde{\rho}_a. \tag{80}$$

   and equations (78).

3. With the r dependence of $\tilde{P}$ and $\tilde{\rho}$ and using (67), we get metric elements $\tilde{m}$ and β up to some functions of u.

4. In order to obtain these unknown functions of u, we integrate *SSE*: (68), (73) and (75). The first two, equations (68) and (73), are model independent, and the third one, (75), depends of the particular choice of the EoS.

5. One has four unknown functions of u for the *SSE*. These functions are: boundary radius A, the velocity of the boundary surface (related to Ω), the total mass M (related to F) and the "total luminosity" L Providing one of these functions, a closure relation and the flux factor f, the *SSE* can be integrated for any particular set of initial data a that fulfill equation (79).

6. By substituting the result of the integration in the expressions for $\tilde{m}$ and β, these metric functions become completely determined.

7. Again, once we have provided a closure relation and the flux factor f, the set of matter variables, ω_x, ρ, P, and $\mathcal{F}$ can be algebraically found for any part of the sphere by using the field equations (36)-(39); rotational physical variables, ω_z and $\mathcal{D}$, can be obtained from the remaining significant, two field equations (43) and (44). Finally, radiations variables, ρ_R and $\mathcal{P}$, emerge from (33), introducing the *flux factor, f*, the *variable Eddington factor* χ and any closure relation.

6. Modelling slowing rotating matter configurations

In order to explore the influence of the dissipation mechanism and the effect of closure relation on the gravitational collapse of slowly rotating matter configurations, we shall work out three models previously studied for spherical (nonrotating) cases. We shall work out three different EoS: *Schwarzschild-like* (Herrera et al 1980; Tolman 1939), *Tolman IV-like* (Aguirre et al 1994; Tolman 1939; Patiño & Rago 1983) and *Tolman VI-like* (Herrera et al 1980; Aguirre et al 1994; Tolman 1939).

6.1. The models we have

The first family of solutions to be considered is the slowly rotating *Schwarzschild-like* model. In the static limit this model represents an incompressible fluid with constant density. It is the same example presented in ref. Herrera et al (1994) but for the present case we have included the flux & Eddington factors (33) and a closure relation from Table 1. The corresponding effective density and pressure can be written as

$$\tilde{\rho} = k(u) = \frac{3}{8\pi}\frac{1-F}{A^2} \quad \text{and} \quad \tilde{P} = k(u)\left\{\frac{3g(u)\left[1-(8\pi/3)k(u)r^2\right]^{1/2}-1}{3-3g(u)\left[1-(8\pi/3)k(u)r^2\right]^{1/2}}\right\}, \tag{81}$$

where the function $g(u)$ can be determined from the boundary condition (80), as

$$g(u) = \frac{3-2\Omega}{\left[1-(8\pi/3)k(u)a^2\right]^{1/2}}. \tag{82}$$

Third surface equation (75) is

$$\dot{\Omega} = \frac{-\Omega}{1-F}\left[\frac{3(1-F)^2(2\Omega-1)(\Omega-1)}{2A\Omega}+\frac{\dot{F}}{F}\right]. \tag{83}$$

The second EoS to be discussed corresponds to the slowly rotating *Tolman-IV-like* model. This model exhibits, in the static limit at the center, the EoS for pure radiation, i.e. $P/\rho \sim 1/3$. The effective density and pressure for this case can be expressed as

$$\tilde{\rho} = \frac{1}{8\pi Z(u)}\left\{\frac{1+3\frac{Z(u)}{W(u)}+3\frac{r^2}{W(u)}}{1+2\frac{r^2}{Z(u)}}+\frac{1-\frac{r^2}{W(u)}}{\left(1+2\frac{r^2}{Z(u)}\right)^2}\right\} \quad \text{and} \quad \tilde{P} = \frac{1-\frac{Z(u)}{W(u)}-3\frac{r^2}{W(u)}}{1+2\frac{r^2}{Z(u)}}; \tag{84}$$

where

$$Z(u) = -\frac{A^2\left[7(1-F)+2\Omega(F-2)-\eta\right]}{2(F-1)(2\Omega+3)}, \tag{85}$$

and

$$W(u) = \frac{-A^2\left(F(1+2\Omega)-1+\eta\right)}{2\left[F(2-3\Omega)+F^2(6\Omega-5)+1+(F-1)\eta\right]}; \tag{86}$$

with

$$\eta = \sqrt{1 + F(22 - 20\Omega) + F^2(4\Omega^2 + 2\Omega - 23)}. \tag{87}$$

For this model, the third surface equation can be written as

$$\dot{\Omega} = \Theta\dot{A} + \Phi\dot{F} + \Gamma \tag{88}$$

where the expression for the coefficients Θ, Φ, and Γ in terms of the *Surface Variables* and their derivatives (i.e. $A, F, \Omega, \dot{A}$,and $\dot{F}$) are sketched in the Appendix.

The third family of models is inspired on *Tolman VI* static solution, which approaches the one of a highly relativistic Fermi Gas, with the corresponding adiabatic exponent of 4/3. For this case we have

$$\tilde{\rho} = \frac{3h(u)}{r^2} = \frac{1}{8\pi r^2}(1 - F) \qquad \text{and} \qquad \tilde{P} = \frac{h(u)}{r^2}\frac{(1 - 9d(u)r)}{(1 - d(u)r)}. \tag{89}$$

As before, the function $d(u)$ is determined from the equation (80), thus, we obtain

$$d(u) = \frac{1}{3}\frac{4\Omega - 1}{A(4\Omega - 3)}. \tag{90}$$

We find that the third surface equation is

$$\dot{\Omega} = \frac{4F^2(F-1)\Omega^3(2\Omega^2 - 5\Omega + 2) + 2\dot{F}A\Omega(\Omega - 1)^2 + F(3 - 2F - F^2)\Omega^2 - F(F-1)^2(1 - 3\Omega)}{2AF(F-1)(\Omega - 1)^2}. \tag{91}$$

6.2. The modeling radiation transfer scenarios

We would like to explore how dissipation affects the dynamics of these three types of slowly rotating matter distributions. For each of the above EoS and several closure relations listed in Table (1), we shall work out simulations with:

1. **Matter configurations with constant *flux factor*** f. We study several radiation transfer environments ranging from the collapse of opaque matter distribution where $f = 0.426$ (close to a *diffusion regime*) to more transparent matter configuration where $f = 0.930$ where the radiation transport mechanism is described near the *free streaming out limit approximation.*

2. **Matter configuration with variable *flux factor*** $f = f(r)$. For this case we study the effect of a variable flux profile as

$$f = f\left(x = \frac{r}{m\,(0)}\right) = \frac{e^{-\zeta(x_t - x)}f_{core} + f_{surface}}{1 + e^{-\zeta(x_t - x)}} \tag{92}$$

on the orbital velocity at the equator. We have defined f_{core} as the flux factor at the inner core and $f_{surface}$ the flux factor at the surface of the distribution. The parameters $x_t = r_t/m\,(0)$

represents the cutoff region where the transition of the dissipation mechanism takes place and ζ regulates how sharp or smooth is the transition between the flux factors at two regions (see Figure 10). The idea with this variable flux factor is to allow configurations with more opaque matter at the inner core and more transparent mass shells at the outer mantle. In many Astrophysical scenarios, radiation diffuses out from a central opaque region ($\chi(f=0)=1/3$) to the transparent boundary ($\chi(f=1)=1$).

6.2.1. General considerations

For all the modelling we perform, we have tried to select a set of initial conditions and physical parameters that resemble, as much as possible, interesting astrophysical scenarios. We have chosen

- Typical values of these conditions that resembles young neutron stars. Notice that because the coupling restriction for slow rotation assumption (59) (or its equivalent in the adimensional variables (79)) the initial radius of the configuration becomes 4 times greater than the typical neutron star radius.
- In our simulations, we have imposed that the energy conditions for perfect fluid be satisfied. In addition, the restrictions $-1<\omega_x,\omega_z<1$ and $r>2\tilde{m}\,(u,r)$ at any shell within the matter configuration are also fulfilled.
- As it was pointed out at the end of the preceding section, the evolution of one of the variable at the surface (boundary radius A, the velocity of the boundary surface (related to Ω), the total mass M (related to F) or the "total luminosity" L) has to be provided. For the present simulation the evolution of the luminosity profile, $L\,(u)$, is given as a Gaussian pulse centered at $u=u_p$

$$-\dot{M}=L=\frac{\Delta M_{rad}}{\lambda\sqrt{2\pi}}\exp\frac{1}{2}\left(\frac{u-u_p}{\lambda}\right)^2, \tag{93}$$

  where λ is the width of the pulse and ΔM_{rad} is the total mass lost in the process. Models has been simulated using

$$\Delta M_{rad}=2.00\times10^{-11}\,M(0),\qquad \lambda=0.74\times10^{-3}\text{s},\qquad t_p=1.48\times10^{-3}\text{s}. \tag{94}$$

- Throughout the simulations equations (55) (or equivalently (59) or (79)) are constantly checked in order to verify the validity of the approximation.

6.2.2. modelling Lorentz-Eddington closure relation

We start modelling with Lorentz-Eddington closure relation,

$$\chi(f_{LE})=\frac{5}{3}-\frac{2}{3}\sqrt{4-3f_{LE}^2}\,, \tag{95}$$

We show there how physically reasonable is the behavior of the emerging physical variables for the three EoS. Afterwards, in Section 6.2.3, we proceed to perform the modelling with other closure relations. The Lorentz-Eddington closure relation (95) was initially proposed by C.D. Levermore in the early 80's (Levermore 1984) on the basis of geometrical considerations, for the case of stationary medium. Later, it has been reobtained by other authors from different perspectives, i.e., thermodynamical point of view with maximum entropy principles (Anile et al 1991) and Information Theory with the energy flux taken as a constraint (Domínguez 1997).

For the modelling with the Lorentz-Eddington closure relation and the three above mentioned EoS we have set initial conditions and parameters to have the following values:

$m(0) =$	$1.0 M_{\odot}$	$\alpha =$	10^{-3}
$A(0) =$	$6,000$	$\Rightarrow a\,(0) \equiv r_{Surface} =$	$44,500\,m$
$\Omega(0) =$	0.999	$\Rightarrow \omega_a\,(0) =$	$-0.00101\,c$

Constant flux factor f Figures 2 through 9 display the profiles of the physical variables: hydrodynamic density, ρ, hydrodynamic pressure, P, radial velocity, ω_x, energy flux, $\mathcal{F}$, radiation density, ρ_R, radiation pressure, $\mathcal{P}$, equatorial orbital velocity, ω_z,and the dragging function $\mathcal{D}$ at the equator.

The effect of the variation of a *constant* flux factor, f, on the evolution of the physical variables is captured, at three different Bondi retarded times, $u = 10, 30, 50$, for the three "seed" equations of state, namely: Schwarzschild-like ($f = 0.426, 0.550, 0.750$ and 0.850), Tolman IV-like ($f = 0.426, 0.550, 0.750$ and 0.850) and Tolman VI-like ($f = 0.850, 0.900$ and 0.930). In the case of the Schwarzschild models it has been obtained that the more diffusive the model is ($f \to 0 \Rightarrow \chi \to \frac{1}{3} \Rightarrow \mathcal{P} \to \frac{1}{3}\rho_R$ i.e. more diffusive configurations), the higher the values of the hydrodynamic density and pressure we get (see plates A-1, A2 and A-3 in figures 2 and 3, respectively). From plates B-1, through C-3 in the same figures, it is clear that the opposite is found for the Tolman-like models. The singularity at the center in the static Tolman VI seed EoS is inherited by the corresponding effective variables (89) and by the resulting hydrodynamic density and pressure (see plates C-1, C2 and C-3 in figures 2 and 3).

Despite the similarity of the evolution for the radial velocity profiles in Schwarzschild-like and Tolman IV-like models where outer layers collapse faster than the inner ones (see Figure 4), the change in the flux factor, f, suggests that both Tolman IV-like and Tolman VI-like models, behave similarly in the sense that lower flux factors imply faster collapsing mass shells. This effect is sharply clear for the Tolman VI-like model (plates C-1, C2 and C-3 in Figure 4) but in this case the core is collapsing faster than the mantle. Again the singularity of this model inhibits the possibility to measure the velocity near the center of the distribution and seems to be responsible of this particular velocity profile.

Again, matter shells for Schwarzschild-like models absorb radiation while emissions registered

for the same shells in the case of Tolman-like models (Figure 5). It is clear that, for Tolman IV-like models (plates C-1, C-2 and C-3), layers near $r/a \sim 1/2$ present the higher emissions and in the case of Tolman VI-like models there are greater energy fluxes at the core of the distribution. The remaining radiation variables such as ρ_R, and $\mathcal{P}$, mimics the behavior of $\mathcal{F}$ (see figures 6 and 7) because the radiation energy density ρ_R, and the radiation pressure, $\mathcal{P}$, profiles are solved, through the flux factor, f, and the closure relation $\chi = \chi(f)$ (95), from the energy flux density, $\mathcal{F}$. The response of radiation energy flux density to a variation of the flux factor between the Schwarzschild-like and Tolman-like models coincides with its effect on the hydrodynamic variables.

The angular variables i.e. equatorial orbital velocity, ω_z,and the dragging function $\mathcal{D}$ at the equator are displayed in figures 8 and 9, respectively. It is clear from figures 8 that in all our models, for the three EoS considered, the core rotates much faster than the envelope and the lower the flux factor we have, the slower the rotation is. These effect seems to be independent of the EoS, at least for the three static "seed" equations of state we have worked out.

Variable flux factor $f = f(r)$ The second, and more realistic, scenario is outlined in Figure 11 where the tangential velocity displayed. The set of parameters corresponding equation (92) are:

$$f_{surface} = 1; \qquad f_{core} = 0.902; \qquad \zeta = 10 \qquad \text{and} \qquad r_t = 14,833m \tag{96}$$

concerning the Schwarzschild-like and Tolman IV-like models, and changing $f_{core} = 0.952$ for the Tolman VI-like models. Because we are interested to study the influence of the dissipation on the rotating collapse we shall only display here figures related to the tangential velocity ω_z. The interested reader is referred to
http://webdelprofesor.ula.ve/ciencias/nunez/CalculosIntermedios/EddintonFactor/Graficas.html
to see the complete set of figures for all physical variables corresponding every EoS in this scenario.

Again we have models with differential rotation but for all EoS considered with a variable flux factor, we have found that, the velocity of the outer layers increases and this effect is more evident for the Tolman VI-like models (plates C-1, C-2 and C-3).

6.2.3. modelling other closure relations

Again, for this modelling we shall also only display figures related to the tangential velocity ω_z. Interested reader is referred to
http://webdelprofesor.ula.ve/ciencias/nunez/CalculosIntermedios/EddintonFactor/Graficas.html
to see the complete set of figures for all physical variables corresponding every EoS in each scenario.

The set of initial conditions and parameters for the modelling performed with the above seed EoS are:

$m(0) =$	$1.0 M_{\odot}$	$\alpha =$	10^{-3}
$A(0) =$	$41,104$	$\Rightarrow a(0) \equiv r_{Surface} =$	$36,500\ m$
$\Omega(0) =$	0.999	$\Rightarrow \omega_a(0) =$	$-0.00101\, c$

We first considered different values for the constant flux factor, f. Figures 12, 13 and 14 display the profiles for the orbital velocity, ω_z, corresponding to Minerbo, Monte Carlo and Maximum Packing closure relation, respectively. The profiles for the same physical variable, ω_z, but corresponding to the variable flux factor $f = f(r)$ are represented in figures 15, 16 and 17 corresponding to the same closure relations.

As in the case studied above (i.e. Lorentz-Eddington) all the other closure relations considered and displayed in figures 12,through 14 represent configurations with differential rotation and where more transparent mass shells rotate faster than the opaque ones. Concerning the variable flux factor for the other closure relations we have found that for Minerbo and Janka closure relations counter rotating mass shells are present near the core of the configuration (figures 15 and 16). This effect does not appear for the above considered Lorentz-Eddington (figure 11) and for the Maximum Packing (figure 17)

7. Summary of results, comments and conclusions

We have extended a previous work (Herrera et al 1994) to study the collapse of a radiating, slow-rotating and self-gravitating relativistic configuration by introducing the *flux factor*, the *Variable Eddington Factor* (equations (33)) and several closure relations displayed in Table 1. Now, it is possible to implement the seminumerical approach to simulate the collapse of distributions where the matter-radiation interaction ranges from near the pure diffusion approximation, $f \sim 0 \Rightarrow \rho_R \sim 3\mathcal{P}$ and $\mathcal{F} \sim \hat{q}$, up to the free streaming out limit: $f \sim 1 \Rightarrow \rho_R \sim \mathcal{F} \sim \mathcal{P} \sim \hat{\epsilon}$. This approach could be useful as an evaluation testbed for emerging full-numerical environments describing general relativistic radiating gravitational collapse. The idea is to "generalize" relatively simple nonstatic models and to analyze some of the essential features from realistic situations that numerical solutions could hinder. As an example we have explored the influence of the dissipation due to the emission of massless particles upon the evolution of some relativistic rotating matter configurations.

The obtained models represent physically reasonable relativistic objects not only because the order of magnitude for values of the parameters considered, but mainly due to the physically reasonable behavior of the emerging physical variables sketched in figures 2-11. Because the very strong coupling restriction imposed by the slow rotation assumption (59), the most plausible astrophysical scenario describing relativistic rotating compact objects surrounded by an "atmospheres" are the models corresponding to Tolman VI-like seed EoS (plates C-1, C2 and C-3 in figures 2 through 11). In spite of its singularity at $r \to 0$, this models could represent objects having hydrodynamic densities $\rho \sim (10 - 20)\rho_0$ at a core $0 < r \lessapprox 10\,\text{Kms.}$ with a thinner matter distribution ($\rho \lessapprox 10^{16}$

gr/cm^3) at the outer mantle $10\,\mathrm{Kms.} \lessapprox r \lessapprox 40\,\mathrm{Kms}$. Schwarzschild-like and Tolman IV-like models (plates A-1, through B-3 in the same figures) provide the same range for hydrodynamic densities, but for configurations having radius 4 times greater than typical ones for neutron stars.

We have found from our simulations the obtained models are extremely differentially rotating matter configurations (the core rotates much faster than the envelope). But more important than this, is the effect of the dissipation on the orbital velocity. From figures 8, 12, 13 and 14 it can be appreciated that the more diffusive the model is, the slower it rotates. These effect seems to be independent of closure relation and also EoS independent, at least for the three static "seed" equations of state we have worked out.

There are two other results which also appears to be independent of the EoS. The first result comes from the continuity of the *first* and the *second fundamental* (g_{ij} and K_{ij}) forms across the matching surface which are fulfilled up to this order of approximation. Considering equation (60), if we assume the flux and the variable Eddington factor for the one dimension case (33), all closure relations listed in Table (1) and we require that the hydrodynamic pressure have to be positive, then the junctions conditions implies that total diffusion regime can not be attained at the surface of the configuration. This result valid, not only for axisymmetric configurations but also for spherical distribution an it is independent of the EoS of the matter configuration. The crucial point becomes the closure relations considered in Table (1), but all of them, obtained by different methods, show this behavior.

The second result emerges from the eccentricity of the configuration considered which are also related to the junctions conditions. From equation (63) it is clear that the eccentricity at the surface of radiating configurations (up to first order in $\tilde{\alpha}$) is greater for models near the diffusion limit approximation than for those in the free streaming out limit. Again, this result is EoS independent and is present for all closure relations we have studied.

Rotation in General Relativity is considered in the slow approximation limit, i.e., situations where the tangential velocity of every fluid element is much less than the speed of light and the centrifugal forces are little compared with the gravitational ones. It is clear from newtonian theory that the effects of rotation on the dynamics are purely relativistic and manifest through the dragging of local inertial frames. It can be understood recalling that the newtonian parameter measuring the "strength" of rotation is not linear in the angular velocity but proportional to the square of it. When the junction conditions are considered, this approximation seems to be very restrictive at least for some type of EoS. Because of equations (56), a combination of significant physical variables, is forced to maintain the order of the approximation. We intuit that this is the reason of the similarity between the two Tolman-like models, and their differences with Schwarzschild-like models, when they become more diffusive. This hypothesis has to be further explored with other seed EoS.

Special attention has to be payed when considering the physics which emerges from a particular closure relation. We have found models where counter rotation is present for some mass shells

surrounding the nucleus. It seems to be an artifact for the closure relation considered (in this case Minerbo and Monte Carlo).

Finally, we would like to end this work with the following comment. Because ultradense matter is not "available" in any earth laboratory, all "known" equations of state, independently of how "elaborated" is the micro-physics they use, emerge from a not very well justified extrapolations and speculations. In any case, the most plausible situation for this "micro-physical description", if any, are static and non-radiating

8. Acknowledgments

We gratefully acknowledge the financial support of the Consejo de Desarrollo Científico Humanístico y Tecnológico de la Universidad de Los Andes under project C-1009-00-05-A, and to the Fondo Nacional de Investigaciones Científicas y Tecnológicas under project S1-2000000820. Two of us (F.A. and T.S.) have been benefited by the computational infrastructure and consulting support of the Centro Nacional de Cálculo Científico, Universidad de Los Andes (CeCalCULA).

9. Appendix

As we have stated in Section 6, the third surface equation for the slowly rotating *Tolman-IV-like* model can be written as

$$\dot{\Omega} = \Theta \dot{A} + \Phi \dot{F} + \Gamma$$

where the expression for the coefficients Θ, Φ, and Γ in terms of the *Surface Variables* are:

$$\Theta = \frac{\Omega}{2A\mathcal{U}} \left\{ 2\Omega^2 F \left(12\Omega^2 F + 22F + \mathcal{H} - 30 \right) - \Omega \left(149F^2 + 146F - 3\mathcal{H}F + 3 - \mathcal{H} \right) + 92F^2 - 88F - 4 \right\}$$

$$\Phi = -\frac{1}{2} \frac{\Omega}{F\mathcal{Q}} \left\{ 2\Omega^2 F^2 (6\Omega F - 4\Omega + 22F + \mathcal{H} - 47) + 3 + \mathcal{H} + \Omega(44\Omega F - 149F^3 - 3F^2\mathcal{H} + 257F^2 - 106F - 2) + F(92F - 157F - \mathcal{H} + 62) \right\}$$

with

$$\mathcal{U} = \Omega F \left[4\Omega F \left(\Omega + 4 \right) - 22\Omega - 63F + 62 \right] + \Omega + 2F \left(23F - 22 \right) - 2,$$

$$\mathcal{Q} = \Omega F \left[4\Omega F \left(\Omega F - \Omega + 4F \right) - \left(38F - 22 \right) \Omega - \left(63F - 125 \right) F - 61 \right] - \Omega + F \left(46F^2 - 90F + 42 \right) + 2$$

and

$$\mathcal{H} = \sqrt{1 + 22F - 20\Omega F - 23F^2 + 20\Omega F^2 + 4\Omega^2 F^2};$$

finally

$$\Gamma = \sum_{k=0}^{5} c_k \Omega^{(k)}$$

where

$$c_0 = 96\pi A^3 F(2F-1)(F-1)$$

$$\begin{aligned} c_1 = 2AF((&-8F\mathcal{T}L + 6F^2 + 4\mathcal{T}L - 9 + 3F)\mathcal{H} + \\ &+ 108F - 267F^2 + 150F^3 + 9 - 4\mathcal{T}L(3F - 2F^2 - 1) \\ &+ \pi A^2(-576F^2 + 864F - 288)) \end{aligned}$$

$$\begin{aligned} c_2 = (&6F^3 + 24AF^3 + 60AF + 12F - 3 - 15F^2 - 84AF^2)\mathcal{H} \\ &+ \pi A^3 F(2112F^2 - 3168F + 1056) - 588AF^2 - 48AF \\ &- 888AF^4 + 1524AF^3 - 3 - 16\mathcal{T}LF^2A(2F-1) \\ &+ F(66F^3 + 117F - 21 - 159F^2) \end{aligned}$$

$$\begin{aligned} c_3 = 6(F-1)(&-16AF^2 + 2F + 8AF - 1)\mathcal{H} \\ &+ 6(F-1)(80AF^3 - 34F^3 + 49F^2 - 48AF^2 - 14F \\ &- 96\pi A^3 F(2F+1) - 4AF - 1) \end{aligned}$$

$$c_4 = -12F(2F-1)(F-1)\mathcal{H} + 12F(2F-1)(F-1)(5F + 8AF - 6)$$

and

$$c_5 = 24F^2(+1 + 2F^2 - 3F)$$

with

$$\mathcal{T} = \frac{1}{2f} - \frac{3}{2}\frac{\chi}{f} + 1 \qquad \text{and} \qquad L = 4\pi A^2(2\Omega - 1)\epsilon.$$

REFERENCES

Aguirre, F., Hernández, H. and Núñez L.A. 1994, Ap&SS, 219, 153.

Ali G. and Romano V. 1994, J. Math.Phys., 35, 2878.

Anderson J.L. and Spiegel E.A. 1972, ApJ, 171, 127.

Anile, A. M. Pennisi, S. and Sammartino, M. 1991, J. Math.Phys., 32, 544.

Barreto,W., Martínez, H. and Rodríguez B., 2002 Ap&SS, 282, 581.

Baumgarte, T. W., Shapiro, S. L., and Shibata, M., 2000, ApJ, 528, L29. [Online article]: cited on 1 Nov 1999, http://arXiv.org/abs/astro-ph/9910565

Berti, E., and Stergioulas, N., 2004, MNRAS, 350, 1416. [Online article]: cited on 16 Feb 2004, http://www.arxiv.org/abs/gr-qc/0310061

Berti, E., White, F., Maniopoulou, A. and Bruni, M. 2004, preprint (gr-qc0405146)

Bondi, H., 1964, Proc. Roy. Soc. London, 281, 39.

Bondi, H., Van der Burg, M. G. J. and Metzner, A. W. K., 1962, Proc. R. Soc. London, A269, 21.

Bruenn, S.W., De Nisco, K.R., and Mezzacappa, A. 2001, ApJ, 560, 326. [Online article]: cited on 23 Jan 2001 , http://arXiv.org/abs/astro-ph/0101400

Carmeli, M. and Kaye, M., 1977, Ann. Phys. (N.Y.), 103, 97.

Chinea, F.J. and González-Romero, L.M. 1993, Rotating Objects and Relativistic Physics. Lecture Notes in Physics, Vol 423, Berlin: Springer Verlag.

CACTUS For information see http://www.cactuscode.org

Demianski, M. 1985, Relativistic Astrophysics, in International Series in Natural Philosophy, Vol 110, Edited by D. Ter Haar, (Oxford: Pergamon).

Dimmelmeier, H., Font, J. A., and Mueller, E. 2002, å, 393, 523 [Online article]: cited on 17 Apr 2002, http://arXiv.org/abs/astro-ph/0204289

Domínguez Cascante, R. 1997, Jour. of Phys A, 30, 7707. [Online article]: cited on 9 Sep 1997, http://www.arXiv.org/abs/cond-mat/9709104

Efimov, G.V., von Waldenfels W. and Wehrse R. 1997, J. Quant. Spectrosc. Radiat. Transfer, 58, 355.

Font, J. 2003, Living Rev. Relativity, 6, 4.[Online article]: cited on 25 Dec 2000 http://www.livingreviews.org/lrr-2003-4/ also in [Online article]: cited on 12 May 2003 http://arXiv.org/abs/gr-qc/0003101

Glendenning, N. K. 2000, Compact Stars, (New York: Springer Verlag).

González,C., Herrera, L. and Jiménez J., 1979, J. Math. Phys., 20, 836.

GRAstro3D. The code GR Astro and its documentation can be found at http://wugrav.wustl.edu/Codes/GR3D

Hartle, J.B., and Thorne, K.S. 1969, ApJ, 158, 719.

Hartle, J. B. 1967, ApJ, 150, 1005.

Hartle, J. B., and Thorne, K. S. 1968, ApJ, 153, 807.

Herrera L., Barreto W., Di Prisco A., and Santos N.O. 2002, Phys. Rev. D, D65, 104004 [Online article]: cited on 14 Feb 2002, http://arXiv.org/abs/gr-qc/0202051

Hernández, H., Núñez, L.A., and Percoco, U. 1999, Class. Quantum Grav, 16, 871. [Online article]: cited on 5 June, 1998, http://arXiv.org/abs/gr-qc/9806029

Herrera, L., Hernández, H., Núñez, L.A. and Percoco, U. 1998, Class. Quantum Grav, 15, 187. [Online article]: cited on 2 Oct 1997 http://arXiv.org/abs/gr-qc/9710017

Herrera, L. and Jiménez, J., 1982, J. Math. Phys., 23, 2339.

Herrera, L. and Jiménez, J. 1982, Phys. Rev. D, 28, 2987.

Herrera, L., Jiménez, J. and Ruggeri, G. 1980, Phys. Rev. D, D22, 2305.

Herrera, L., Melfo, A., Núñez, L.A. and Patiño, A. 1994, ApJ, 421, 677.

Herrera, L. and Núñez, L. A. 1990, Fund. Cosmic Phys., 14, 235.

Herrera, L. and Santos N.O. 1997, Phys. Rep., 286, 53.

Kippenhahn, R. and Weigert, A. 1990, Stellar Structure and Evolution, (Springer Verlag, New York).

Kramer, D. and Hahner, U., 1995, Class. Quantum. Grav., 12, 2287.

Levermore C. D. 1984, J. Quant. Spectrosc. Radiat. Transfer, 31, 149.

Liebendörfer, M., Mezzacappa, A., Thielemann, F., *et al.*2001, Phys. Rev. D, 63, 3004. [Online article]: cited on 28 Jun 2000, http://arXiv.org/abs/astro-ph/0006418

Liebendörfer, M, O. E. B., Mezzacappa A. et al, 2002, Preprint (astro-ph/0207036)

Lindquist R. W. 1966, Ann. Phys., 37, 487.

Lorimer, D.R. 2001 Living Rev. Relativity, 4, 5. [Online article]: cited on 15 Aug 2001 http://www.livingreviews.org/lrr-2001-5

Lyford, N.D., Baumgarte, T.W. and Shapiro, S. L. 2003, ApJ, 583, 410 [Online article]: cited on 3 Oct 2002, http://arXiv.org/abs/gr-qc/0210012

Manko, V.S., Mielke, E.W., and Sanabria-Gómez, J.D. 2000, Phys. Rev. D, 61, 081501-1.[Online article]: cited on 23 April 2002, http://www.arxiv.org/abs/gr-qc/0001081 Manko, V.S., Sanabria-Gómez, J.D., and Manko, O.V., 2000, Phys. Rev. D, 62, 044048-1.

Mihalas, D. and Weibel Mihalas, B. 1984, Foundations of Radiation Hydrodynamics (Oxford: Oxford University Press).

NASAGC The NASA Grand Challenge Project is described at http://wugrav.wustl.edu/Relativ/nsgc.html

Ostriker, J. P., Bodenheimer, P, and Lynden-Bell, D., 1966, Phys. Rev. Lett., 17, 816

Patiño, A. and Rago, H. 1983, Lett. Nuovo Cimento, 38, 321.

Pons, J.A. Ibañez, J. M[a] and Miralles J. A. 2000, MNRAS, 317, 550. [Online article]: cited on 15 May 2000, http://arXiv.org/abs/astro-ph/0005310

Rampp M. and Janka H.-Th. 2002 A&A, 396, 361. [Online article]: cited on 7 Mar 2002, http://arXiv.org/abs/astro-ph/0203101

Rezzolla L. and Miller J. 1994, Class. Quantum Grav., 11, 1815.

Shapiro, S.L. and Teukolsky, S.A. 1983, Black Holes, White Dwarfs and Neutron Stars, (New York: John Willey).

Sibgatullin, N.R., and Sunyaev, R.A. 2000, Astron. Lett., 26, 699. [Online article]: cited on 23 April 2002, http://www.arxiv.org/abs/astro-ph/0011253

Siebel, F., Font, J.A., Müller, E., and Papadopoulos, P. 2003, Phys. Rev. D, 67, 124018. [Online article]: cited on 7 February 2003, http://www.arxiv.org/abs/gr-qc/0301127

Smit, J.M.,Van den Horn, L.J., and Bludman, S.A. 2000, A&A, 356, 559.

Stergioulas, N. 2003, Living Rev. Relativity, 6. [Online article]: cited on 25 Dec 2000 http://www.livingreviews.org/lrr-2003-3/ also [Online article]: cited on 10 Feb 2003 in http://arXiv.org/abs/gr-qc/0302034

Tolman, R.C. 1939, Phys. Rev., 55, 364.

Wehrse R. and Vaschek B. 1999, Phys. Rep., 311, 187.

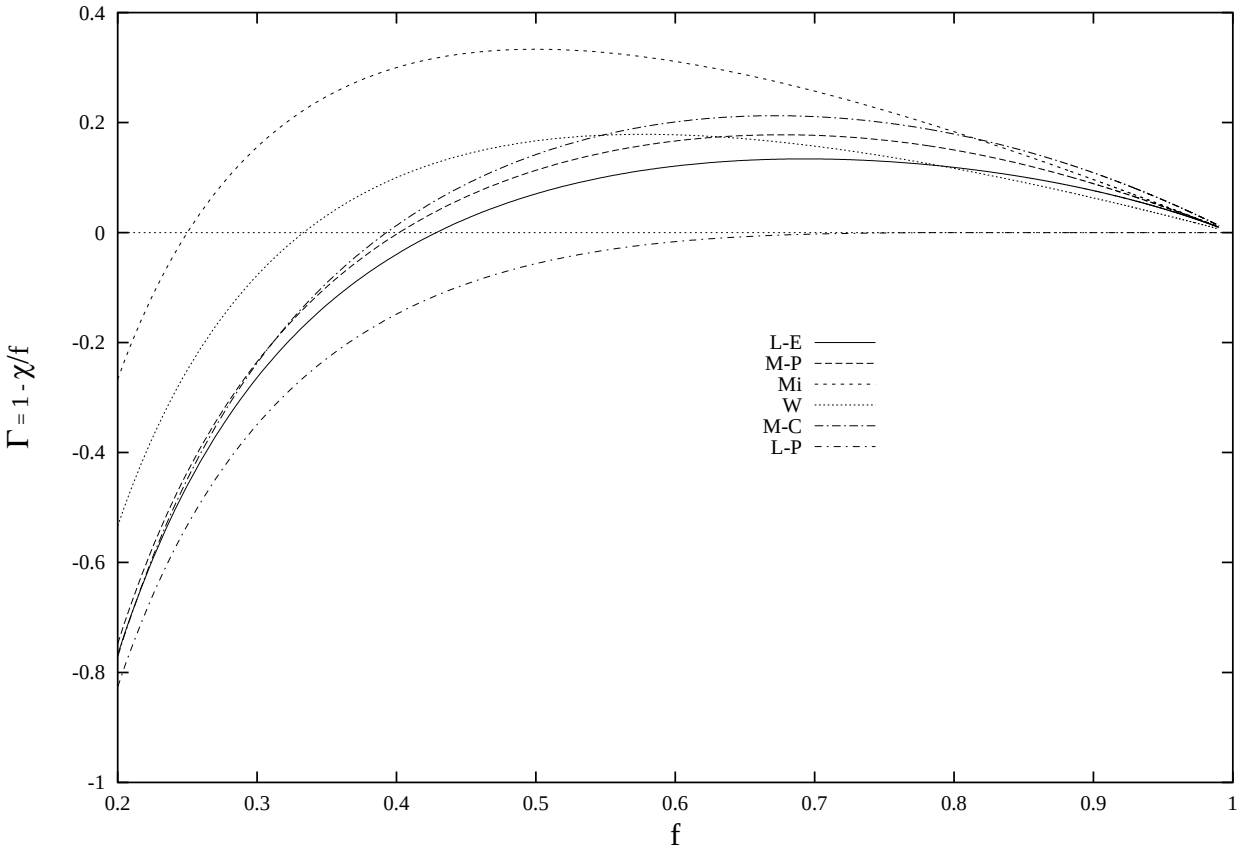

Fig. 1.— The $\left(1-\frac{\chi_a}{f_a}\right)$ vs f for the different closure relations. **L-E**→*Lorentz-Eddington*; **M-P**→*Maximum Packing;* **Mi**→*Minerbo;* **W**→*Bowers-Wilson;* **M-C**→*Janka (Monte Carlo);* **L-P**→*Levermore-Pomraning.*

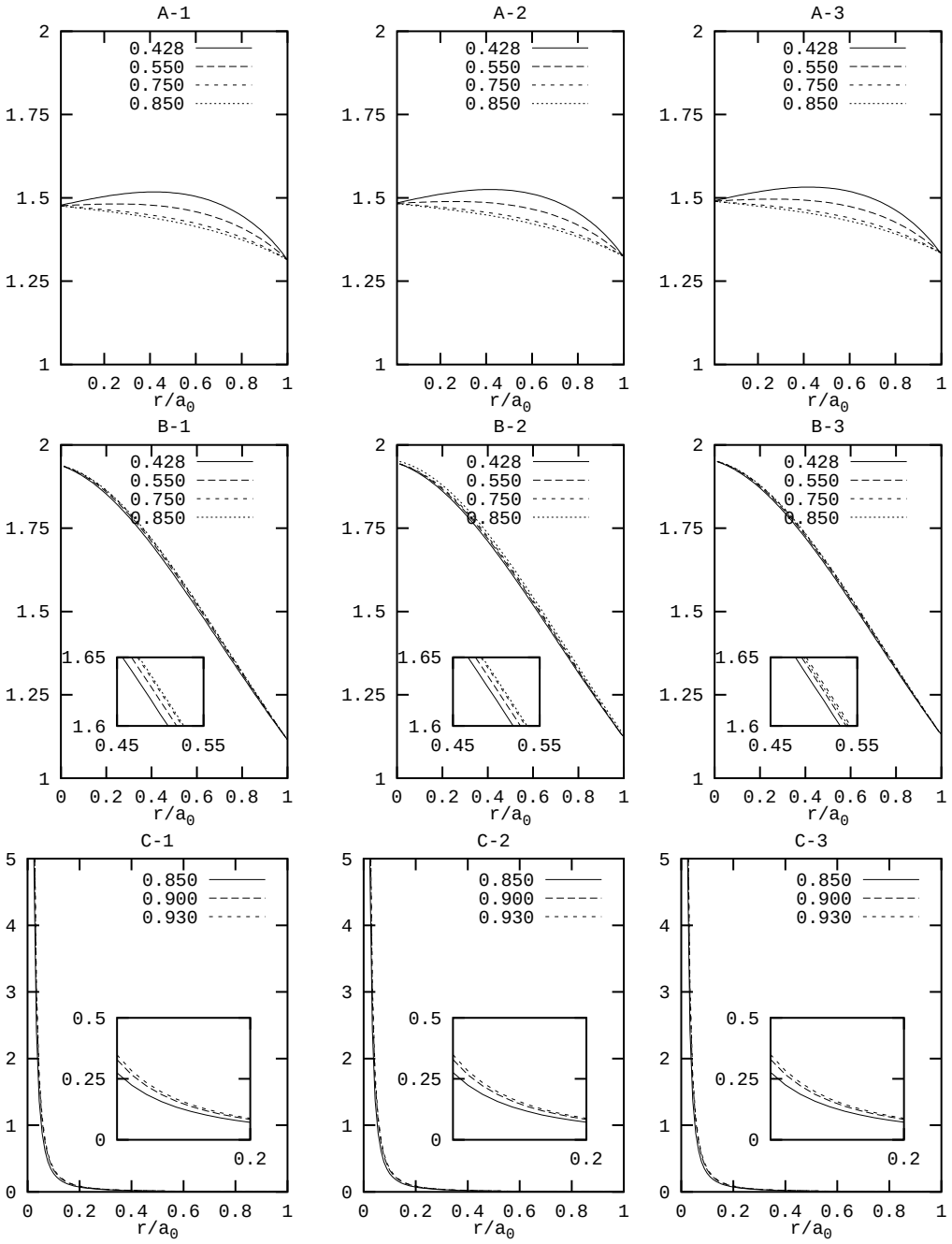

Fig. 2.— Profiles of hydrodynamic density, $\rho \times 10^{14}$ gr/cm^3,corresponding to Schwarzschild-like and for Tolman IV-like are represented in plates A-1 thought A-3 and B-1 thought B-3, respectively. Tolman VI-like models are displayed in plates C-1 thought C-3 as $\rho \times 10^{16}$ gr/cm^3. The various flux factors are $f_{LE} = 0.426, 0.550, 0.750, 0.850$ for Schwarzschild-like and the Tolman IV-like models and $f_{LE} = 0.850, 0.900, 0.930$ for the Tolman VI-like. The retarded times displayed are $u = 10, 30, 50$.

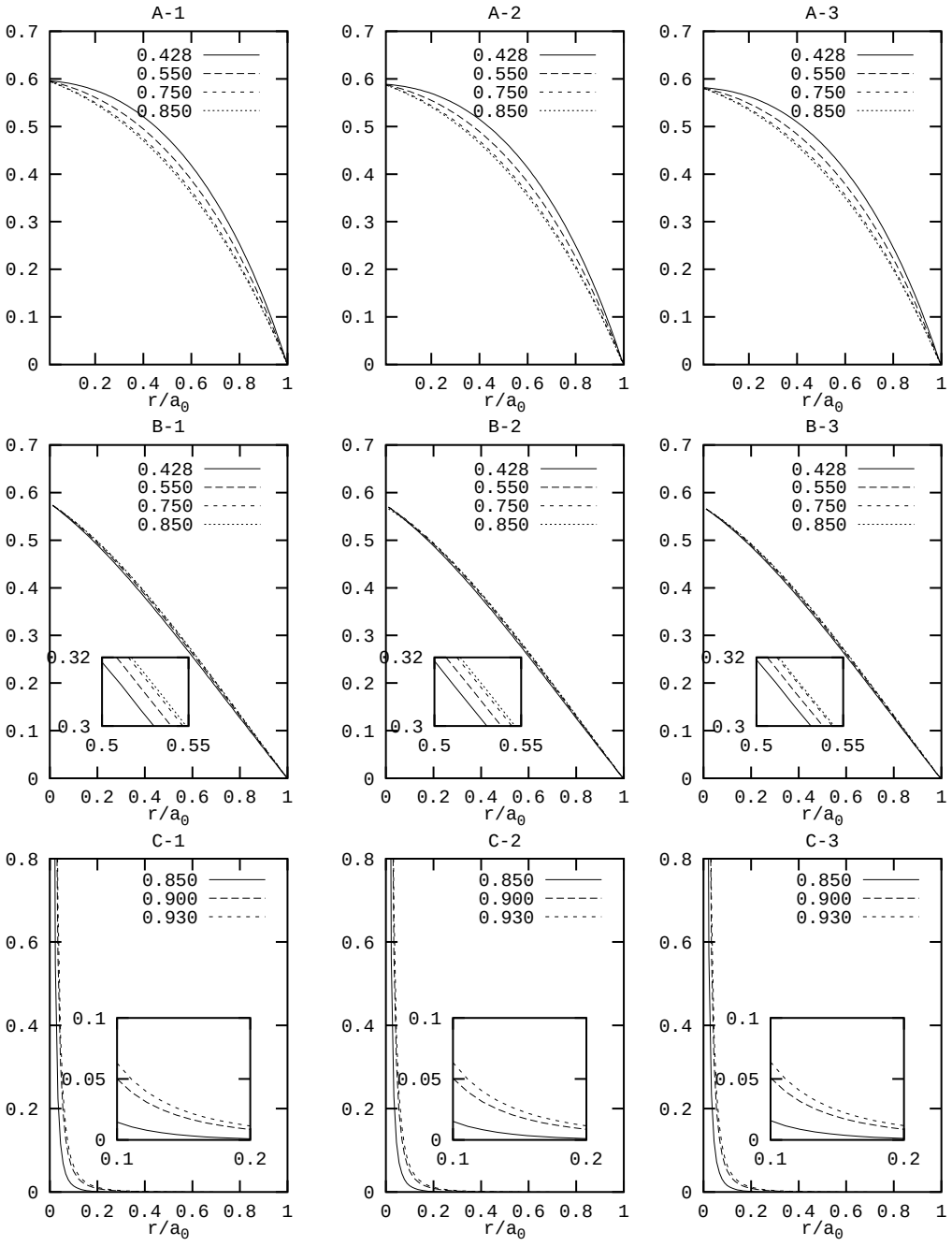

Fig. 3.— Profiles of hydrodynamic pressure, $P \times 10^{40}$din/cm^2 corresponding to Schwarzschild-like and for Tolman IV-like are respresented in plates A-1 thought A-3 and B-1 thought B-3, respectively. Tolman VI-like models are displayed in plates C-1 thought C-3 as $P \times 10^{44}$din/cm^2. The various flux factors are $f_{LE} = 0.426, 0.550, 0.750, 0.850$ for Schwarzschild-like and the Tolman IV-like models and $f_{LE} = 0.850, 0.900, 0.930$ for the Tolman VI-like. The retarded times displayed are $u = 10, 30, 50$.

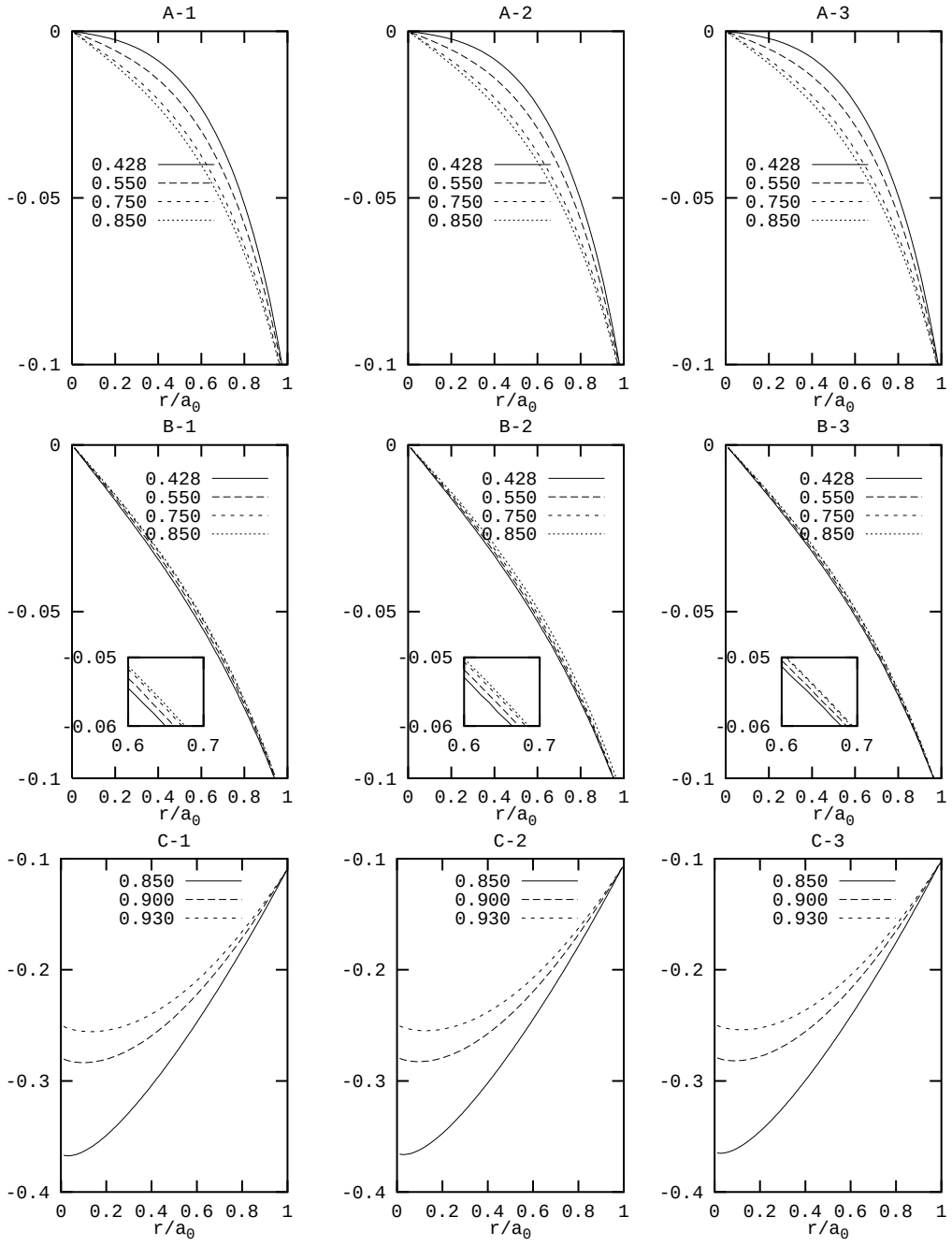

Fig. 4.— Profiles of radial velocity, $\omega_x \times c$, corresponding to Schwarzschild-like for Tolman IV-like and Tolman VI-like are respresented in plates (A-1 thought A-3), (B-1 thought B-3) and (C-1 thought C-3), respectively. The various flux factors are $f_{LE} = 0.426, 0.550, 0.750, 0.850$ for Schwarzschild-like and the Tolman IV-like models and $f_{LE} = 0.850, 0.900, 0.930$ for the Tolman VI-like. The retarded times displayed are $u = 10, 30, 50$.

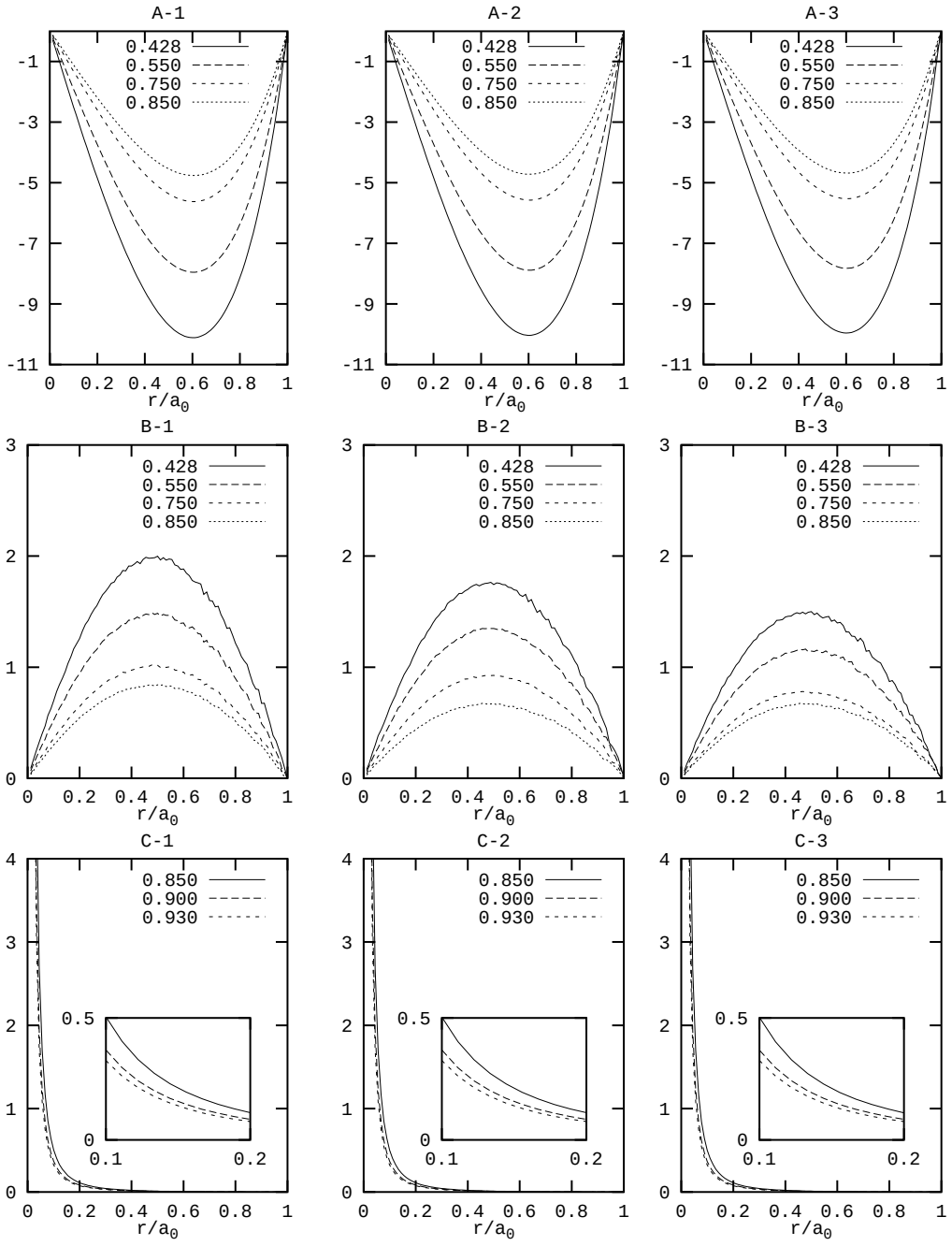

Fig. 5.— Profiles of energy flux density, $\mathcal{F} \times 10^{42}$erg/cm^{2}s corresponding to Schwarzschild-like and for Tolman IV-like are respresented in plates A-1 thought A-3 and B-1 thought B-3, respectively. Tolman VI-like models are displayed in plates C-1 thought C-3 as $\mathcal{F} \times 10^{46}$erg/cm^{2}s. The various flux factors are $f_{LE} = 0.426, 0.550, 0.750, 0.850$ for Schwarzschild-like and the Tolman IV-like models and $f_{LE} = 0.850, 0.900, 0.930$ for the Tolman VI-like. The retarded times displayed are $u = 10, 30, 50$.

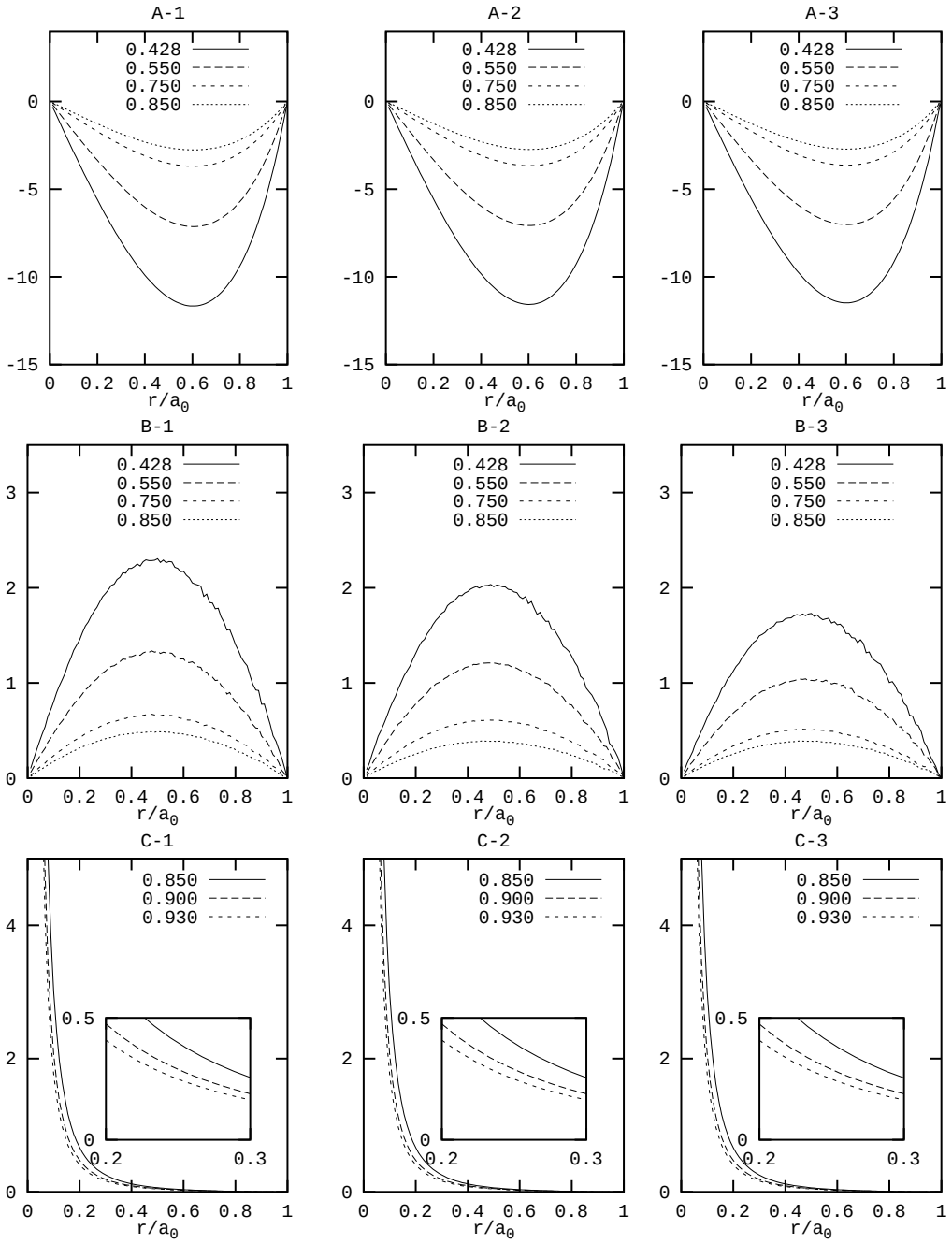

Fig. 6.— Profiles of radiation density, $\rho_R \times 10^{11}$ gr/cm^3,corresponding to Schwarzschild-like and for Tolman IV-like are respresented in plates A-1 thought A-3 and B-1 thought B-3, respectively. Tolman VI-like models are displayed in plates C-1 thought C-3 as $\rho_R \times 10^{13}$ gr/cm^3. The various flux factors are $f_{LE} = 0.426, 0.550, 0.750, 0.850$ for Schwarzschild-like and the Tolman IV-like models and $f_{LE} = 0.850, 0.900, 0.930$ for the Tolman VI-like. The retarded times displayed are $u = 10, 30, 50$.

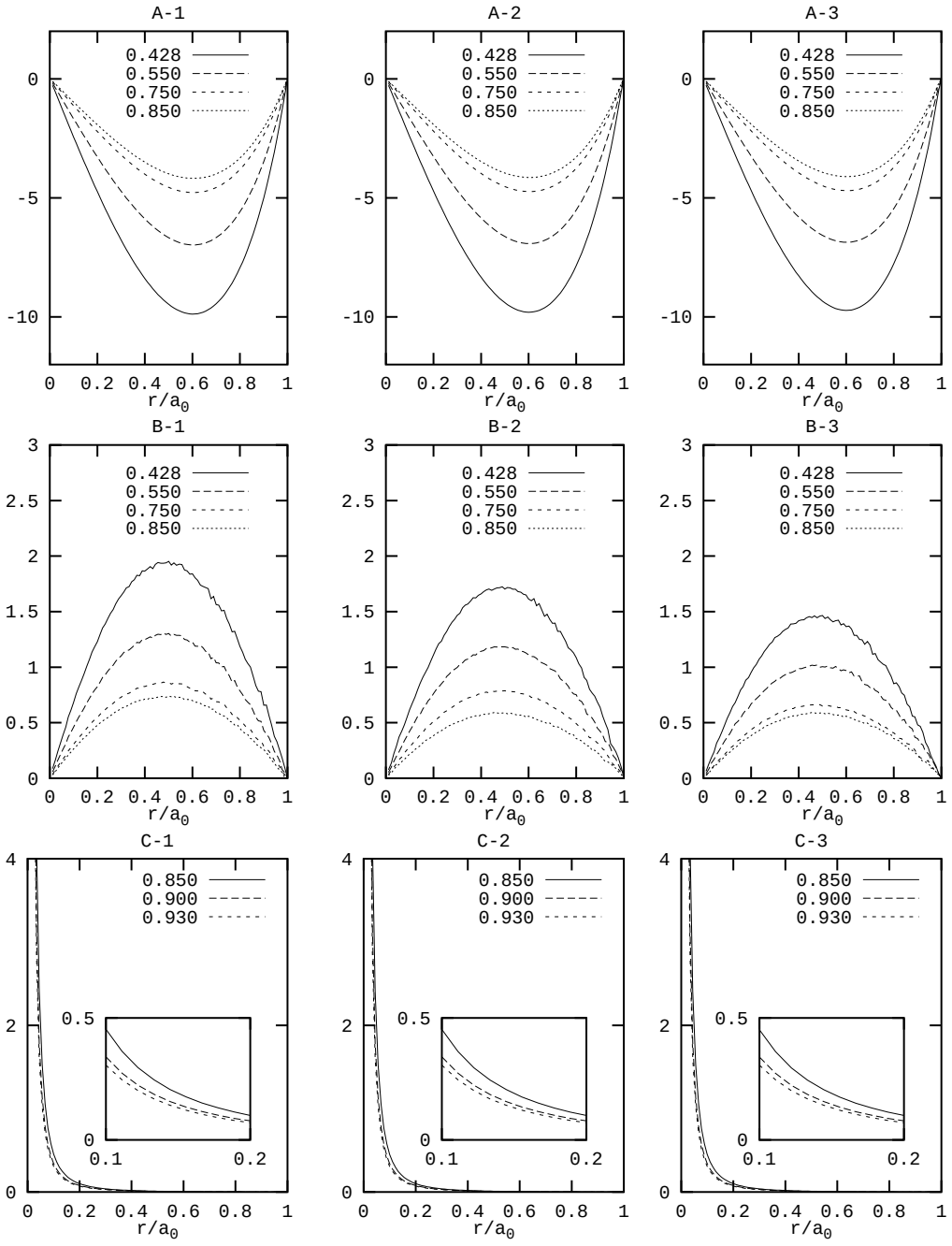

Fig. 7.— Profiles of radiation pressure, $\mathcal{P} \times 10^{38}$din/cm^2 corresponding to Schwarzschild-like and for Tolman IV-like are respresented in plates A-1 thought A-3 and B-1 thought B-3, respectively. Tolman VI-like models are displayed in plates C-1 thought C-3 as $\mathcal{P} \times 10^{42}$din/cm^2. The various flux factors are $f_{LE} = 0.426, 0.550, 0.750, 0.850$ for Schwarzschild-like and the Tolman IV-like models and $f_{LE} = 0.850, 0.900, 0.930$ for the Tolman VI-like. The retarded times displayed are $u = 10, 30, 50$.

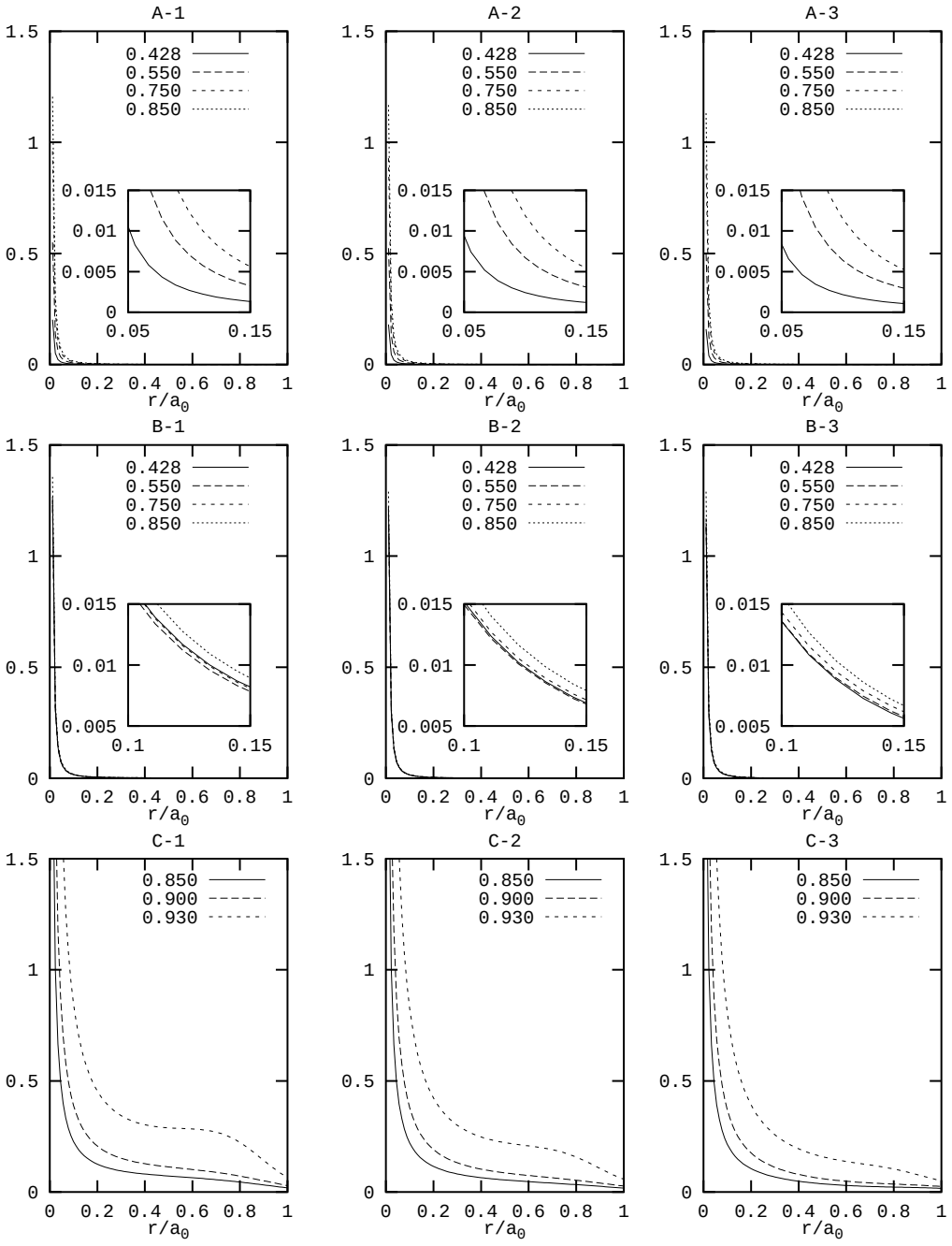

Fig. 8.— Profiles of orbital velocity ω_z $\times 10^{-6}c$, corresponding to Schwarzschild-like for Tolman IV-like and Tolman VI-like are respresented in plates (A-1 thought A-3), (B-1 thought B-3) and (C-1 thought C-3), respectively. The various flux factors are $f_{LE} = 0.426, 0.550, 0.750, 0.850$ for Schwarzschild-like and the Tolman IV-like models and $f_{LE} = 0.850, 0.900, 0.930$ for the Tolman VI-like. The retarded times displayed are $u = 10, 30, 50$.

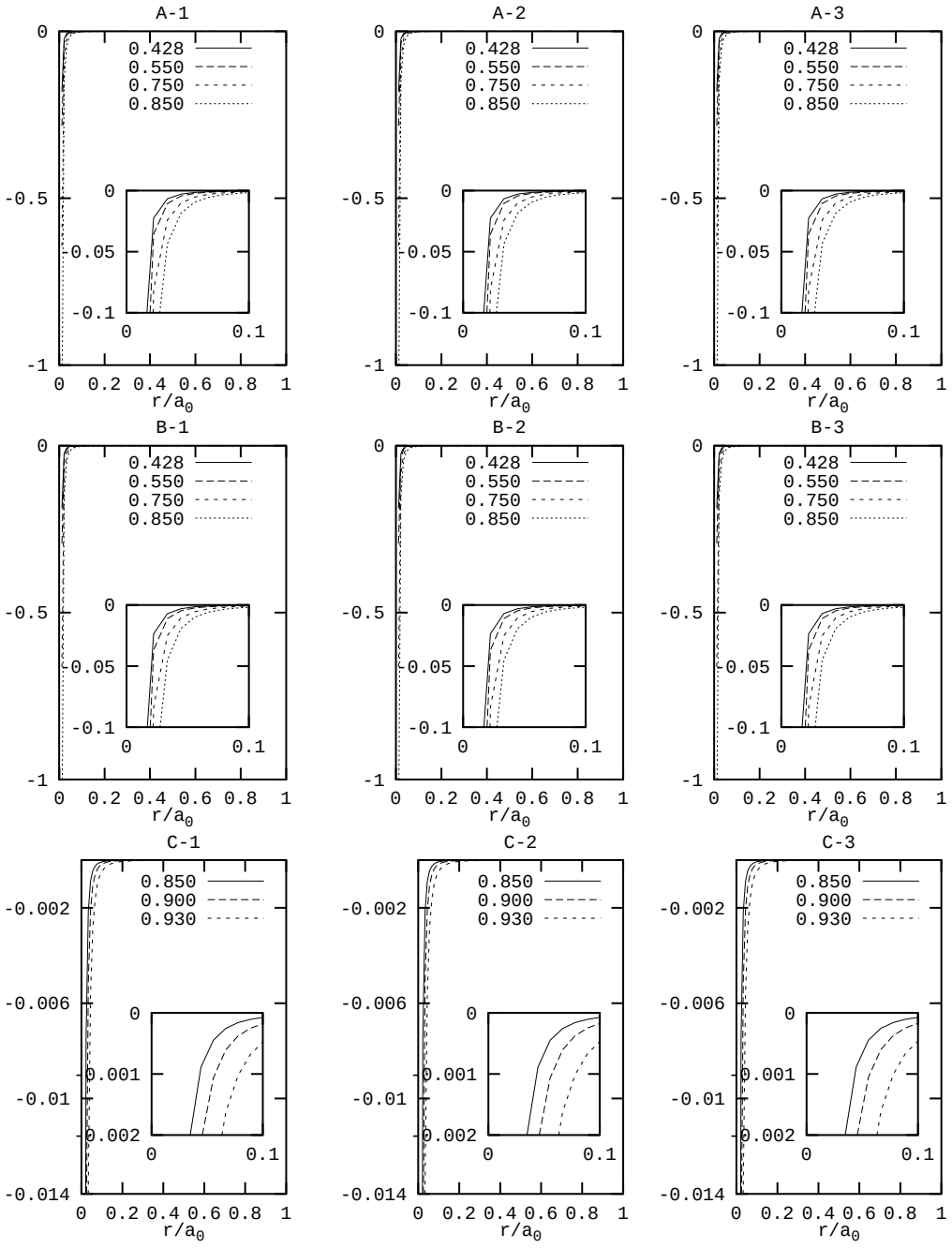

Fig. 9.— Profiles of the dragging function $\mathcal{D} \times 10^{42}$erg/cm^{2}s corresponding to Schwarzschild-like and for Tolman IV-like are respresented in plates A-1 thought A-3 and B-1 thought B-3, respectively. Tolman VI-like models are displayed in plates C-1 thought C-3 as $\mathcal{D} \times 10^{46}$erg/cm^{2}s The various flux factors are $f_{LE} = 0.426, 0.550, 0.750, 0.850$ for Schwarzschild-like and the Tolman IV-like models and $f_{LE} = 0.850, 0.900, 0.930$ for the Tolman VI-like. The retarded times displayed are $u = 10, 30, 50$.

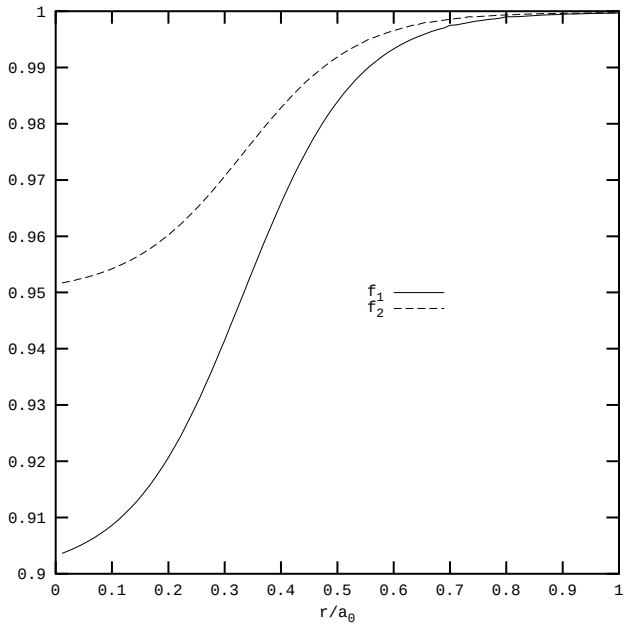

Fig. 10.— Variable Flux factor $f = f\left(x = \frac{r}{m(0)}\right) = \frac{\left(f_{surface} + e^{-\zeta(x_t - x)} f_{core}\right)}{\left(1 + e^{-\zeta(x_t - x)}\right)}$where $f_1 = f_{core} = 0.902$ which is considered the Schwarzschild-like and Tolman IV-like models, and changing $f_2 = f_{core} = 0.952$ for the Tolman VI-like models.

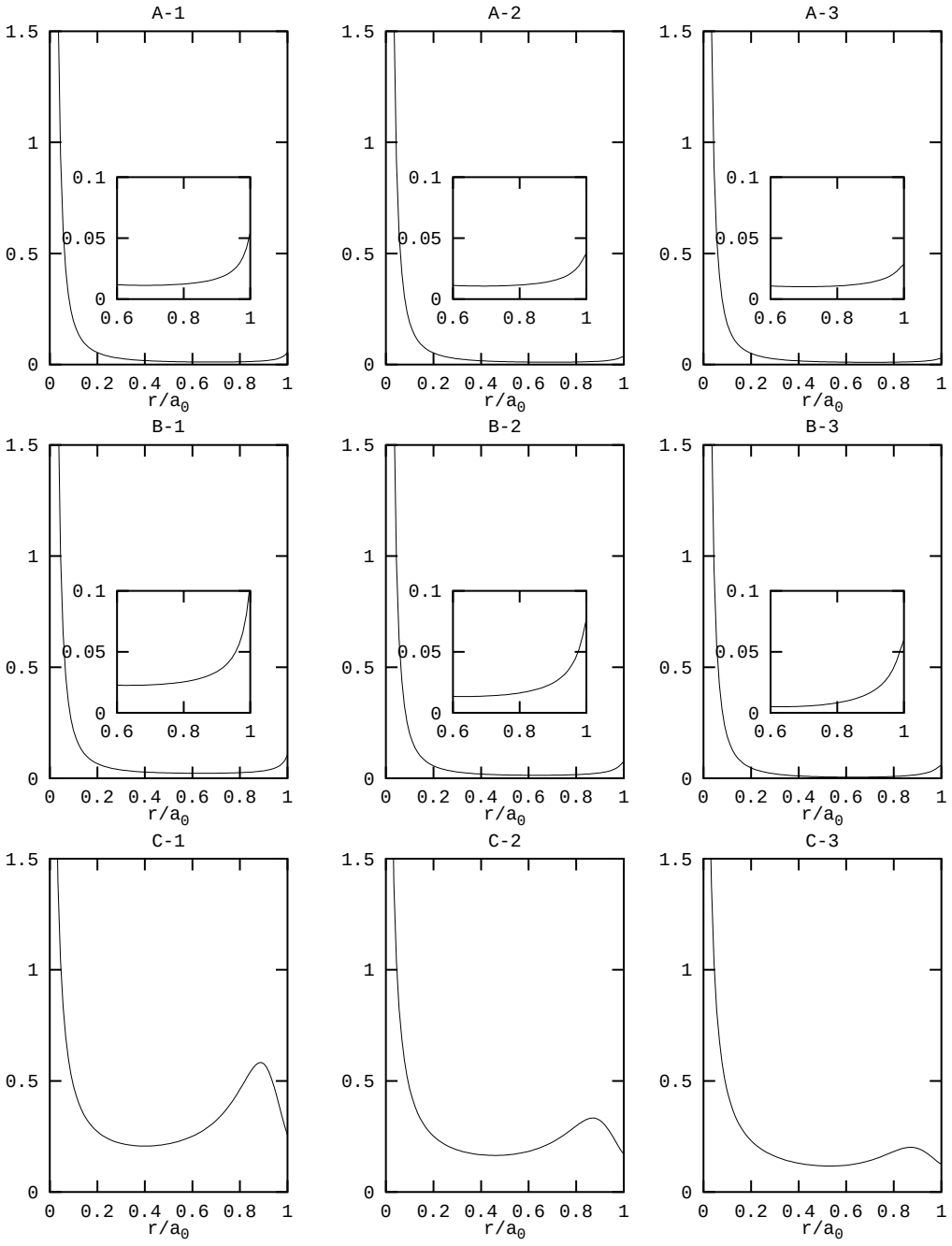

Fig. 11.— Profiles of orbital velocity ω_z $\times 10^{-6}c$, for the Schwarzschild-like (plates A-1 thought A-3), Tolman IV-like (plates B-1 thought B-3) and Tolman VI-like (plates C-1 thought C-3) at three distinct times
$u = 10, 30, 50$. The profiles in each plate correspond to a variable Flux factor
$f_{LE} = f_{LE}\left(x = \frac{r}{m(0)}\right) = \frac{\left(e^{-\zeta(x_t - x)} f_{LE surface} + f_{core}\right)}{\left(1 + e^{-\zeta(x_t - x)}\right)}$.

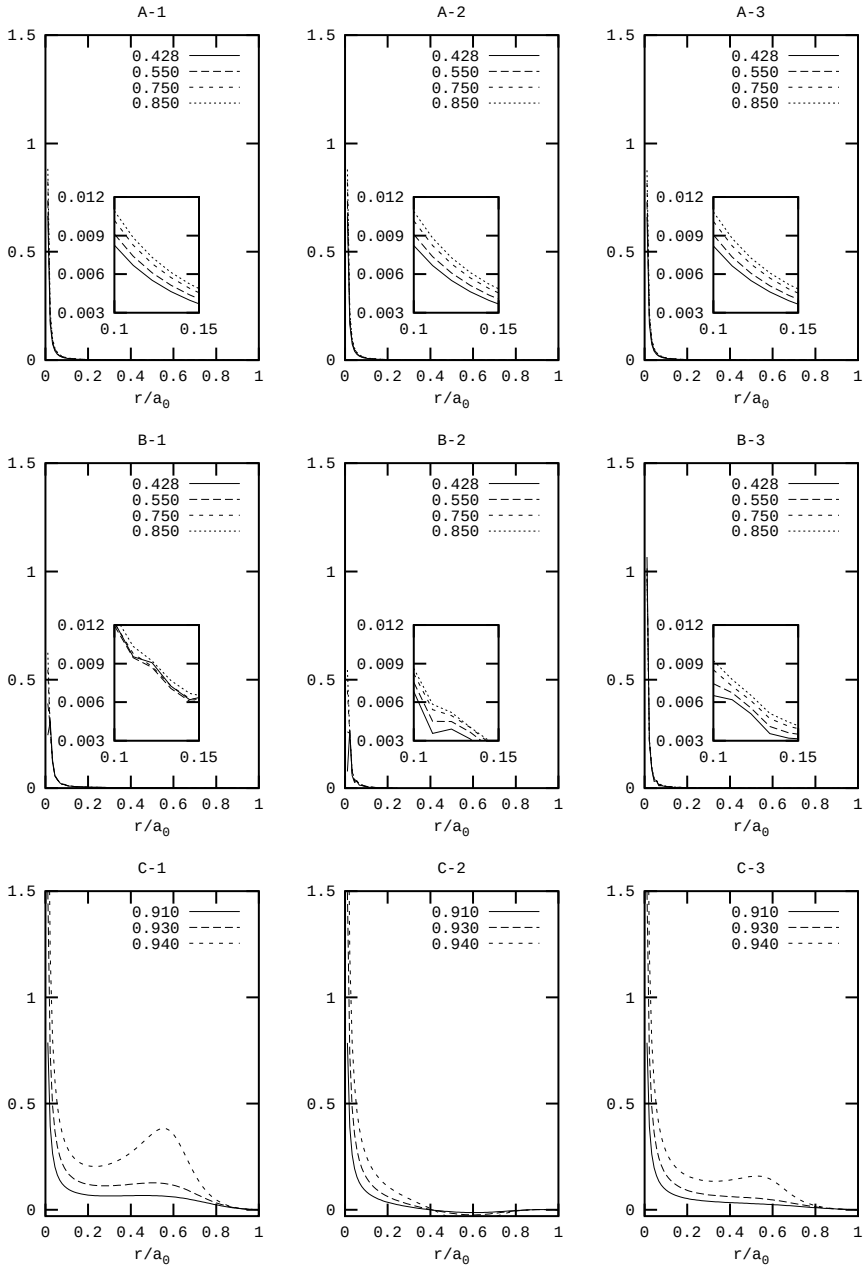

Fig. 12.— Profiles of orbital velocity corresponding to *Minerbo* closure relation. They are represented in A-1 thought A-3 (Schwarzschild-like); B-1 thought B-3 (Tolman IV-like) and plates C-1 thought C-3 (Tolman VI-like) with $\omega_z \times 10^{-5} c$. The flux factors are $f_{Mi} = 0.428, 0.550, 0.750, 0.850$ for Schwarzschild-like and the Tolman IV-like models and $f_{Mi} = 0.910, 0.930, 0.940$ for the Tolman VI-like with $\omega_z \times 10^{-4} c$. The retarded times displayed are $u = 10, 30, 50$.

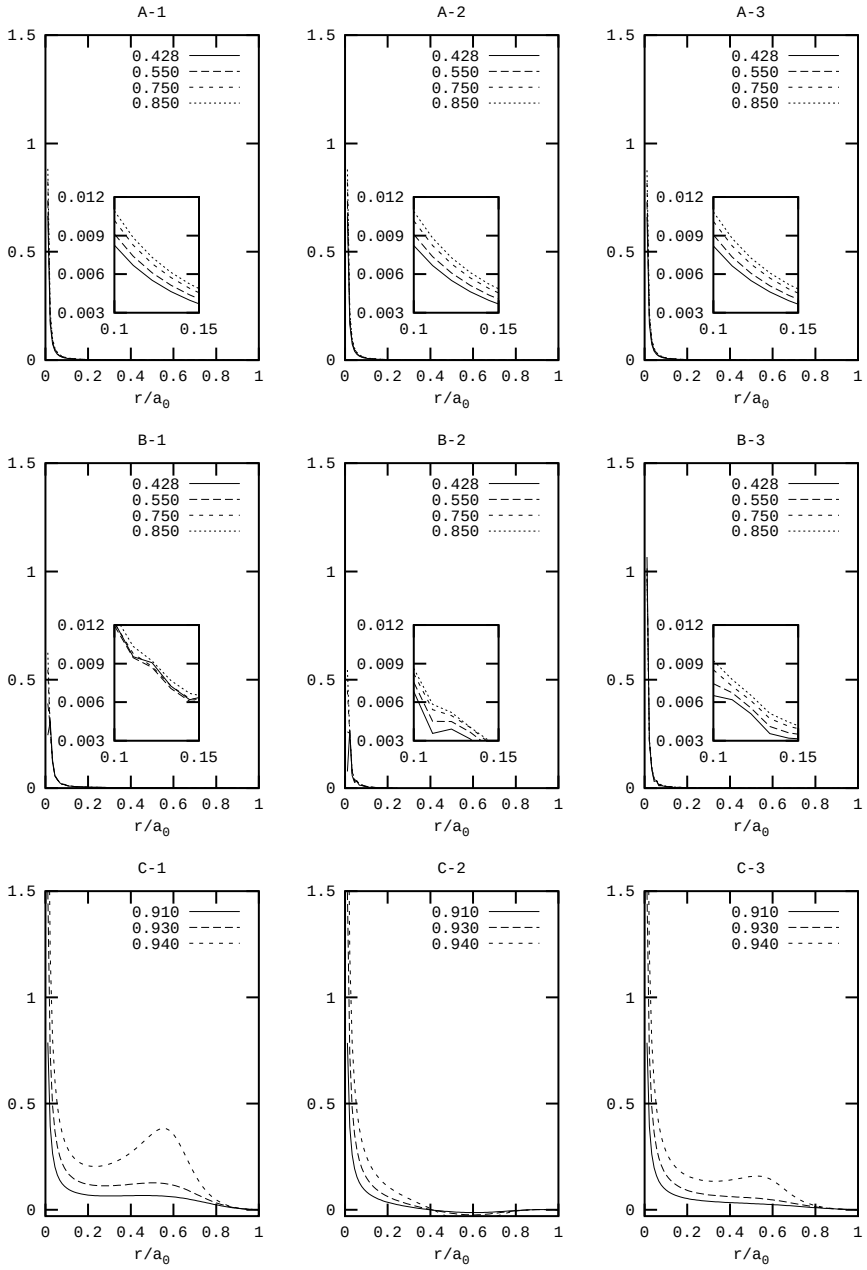

Fig. 13.— Profiles of orbital velocity corresponding to *Janka* (*Monte Carlo*) closure relation. They are represented in A-1 thought A-3 (Schwarzschild-like); B-1 thought B-3 (Tolman IV-like) and plates C-1 thought C-3 (Tolman VI-like) with ω_z $\times 10^{-5}c$. The flux factors are $f_{MC} = 0.428, 0.550, 0.750, 0.850$ for Schwarzschild-like and the Tolman IV-like models and $f_{MC} = 0.910, 0.930, 0.940$ for the Tolman VI-like with ω_z $\times 10^{-4}c$. The retarded times displayed are $u = 10, 30, 50$.

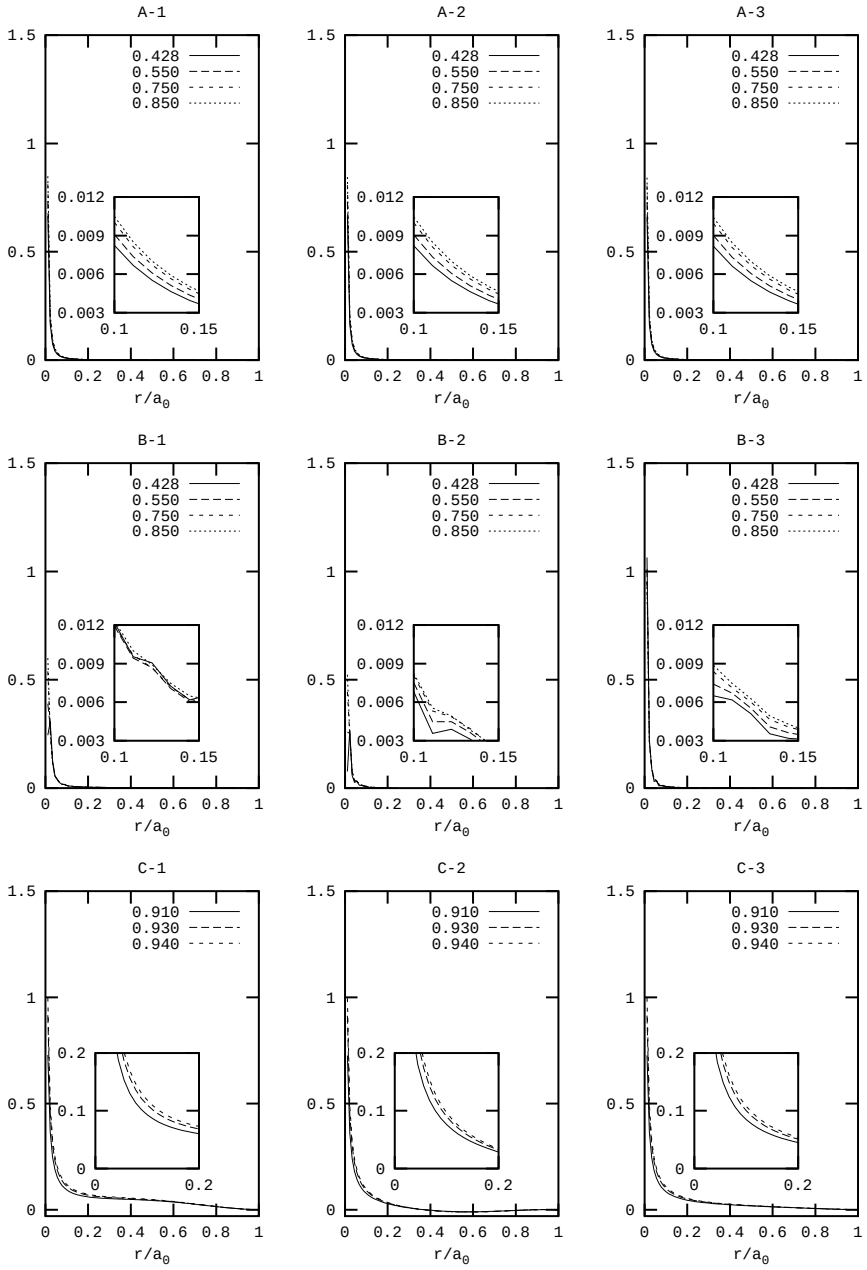

Fig. 14.— Profiles of orbital velocity corresponding to *Maximum Packing* closure relation. They are represented in A-1 thought A-3 (Schwarzschild-like); B-1 thought B-3 (Tolman IV-like) and plates C-1 thought C-3 (Tolman VI-like) with $\omega_z \times 10^{-5}c$. The flux factors are $f_{MP} = 0.428, 0.550, 0.750, 0.850$ for Schwarzschild-like and the Tolman IV-like models and $f_{MP} = 0.910, 0.930, 0.940$ for the Tolman VI-like with $\omega_z \times 10^{-4}c$. The retarded times displayed are $u = 10, 30, 50$.

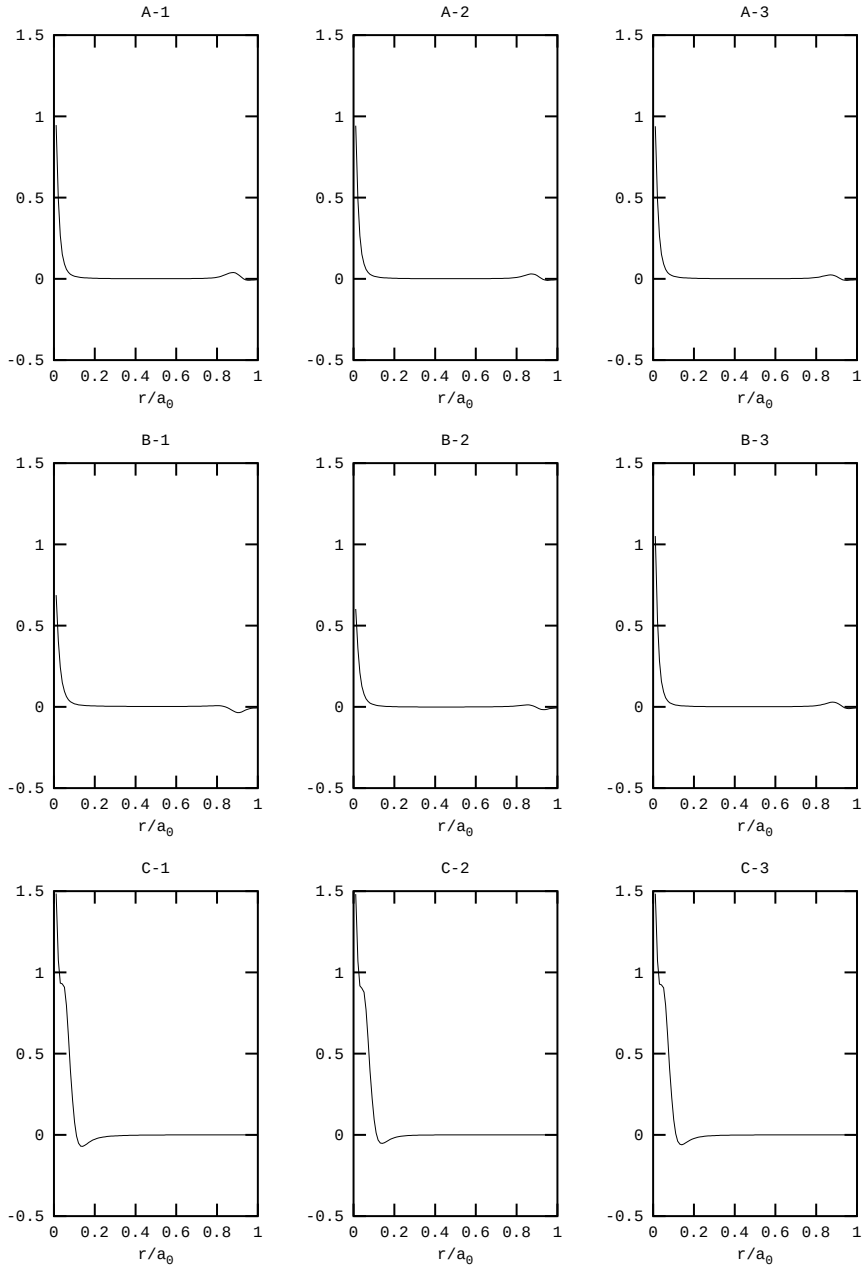

Fig. 15.— Profiles of orbital velocity $\omega_z \times 10^{-6} c$, corresponding *Minerbo* closure relation. They are represented in A-1 thought A-3 (Schwarzschild-like); B-1 thought B-3 (Tolman IV-like) and plates C-1 thought C-3 (Tolman VI-like) at three distinct times $u = 10, 30, 50$. The profiles in each plate correspond to a variable Flux factor $f_{Mi} = f_{Mi}\left(x = \frac{r}{m(0)}\right) = \frac{\left(f_{Misurface} + e^{-\zeta(x_t - x)} f_{core}\right)}{\left(1 + e^{-\zeta(x_t - x)}\right)}$.

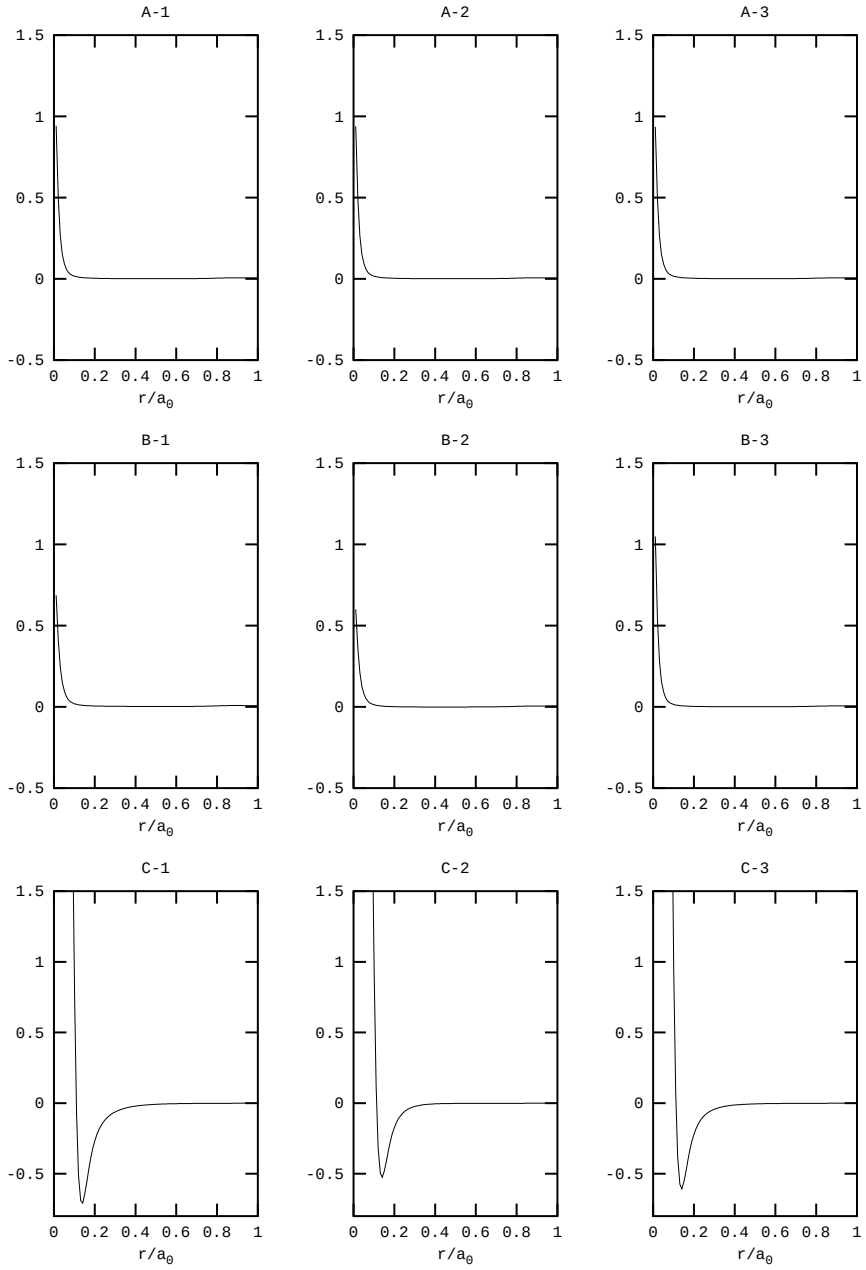

Fig. 16.— Profiles of orbital velocity ω_z $\times 10^{-6}c$, corresponding *Janka* (*Monte Carlo*) closure relation. They are represented in A-1 thought A-3 (Schwarzschild-like); B-1 thought B-3 (Tolman IV-like) and plates C-1 thought C-3 (Tolman VI-like) at three distinct times $u = 10, 30, 50$. The profiles in each plate correspond to a variable Flux factor $f_{MC} = f_{MC}\left(x = \frac{r}{m(0)}\right) = \frac{\left(f_{MC\,surface} + e^{-\zeta(x_t - x)} f_{core}\right)}{\left(1 + e^{-\zeta(x_t - x)}\right)}$.

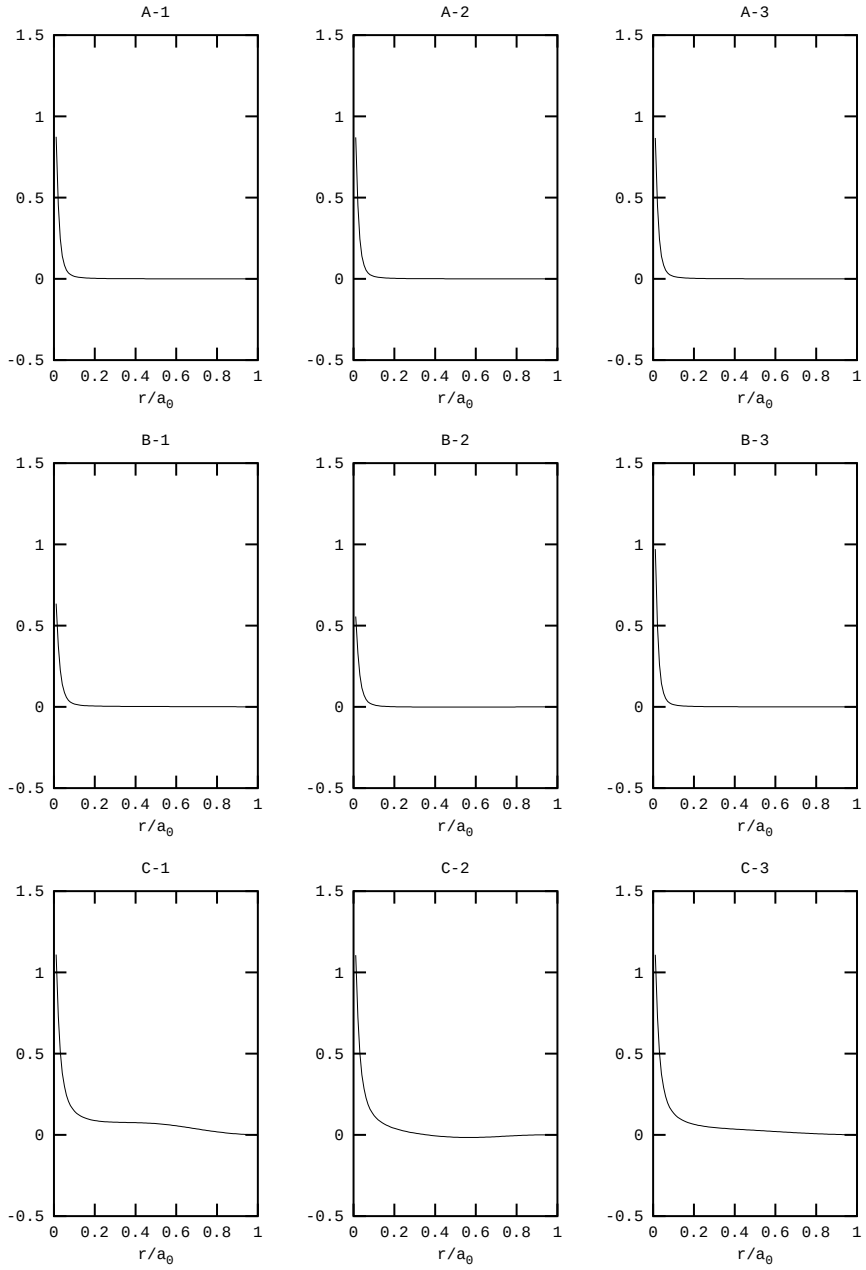

Fig. 17.— Profiles of orbital velocity $\omega_z \times 10^{-6} c$, corresponding *Maximum Packing* closure relation. They are represented in A-1 thought A-3 (Schwarzschild-like); B-1 thought B-3 (Tolman IV-like) and plates C-1 thought C-3 (Tolman VI-like) at three distinct times $u = 10, 30, 50$. The profiles in each plate correspond to a variable Flux factor $f_{MP} = f_{MP}\left(x = \frac{r}{m(0)}\right) = \frac{\left(f_{MPsurface} + e^{-\zeta(x_t - x)} f_{core}\right)}{\left(1 + e^{-\zeta(x_t - x)}\right)}$.

Closure	$\chi(f)$	$\left.\frac{\mathrm{d}\chi}{\mathrm{d}f}\right\|_{f=1}$	$\left.\frac{\mathrm{d}\chi}{\mathrm{d}f}\right\|_{f=0}$
Lorentz-Eddington (LE)	$\frac{5}{3}-\frac{2}{3}\sqrt{4-3f^2}$	2	0
Bowers-Wilson	$\frac{1}{3}\left(1-f+3f^2\right)$	$\frac{5}{3}$	$-\frac{1}{3}$
Janka (Monte Carlo) (MC)	$\frac{1}{3}\left(1+\frac{1}{2}f^{1.31}+\frac{3}{2}f^{4.13}\right)$	2.28	0
Maximum Packing (MP)	$\frac{1}{3}\left(1-2f+4f^2\right)$	2	$-\frac{2}{3}$
Minerbo (Mi)	$\chi(f)=1-2\frac{f}{\kappa}$ where $f=\coth\kappa-\frac{1}{\kappa}$	2	0
Levermore-Pomraning	$\chi(f)=f\coth\beta$ where $f=\coth\beta-\frac{1}{\beta}$	1	0

Table 1: Closure Relations and some of their physical acceptability conditions

Closure	$f_{r=a}$	e
Lorentz-Eddington	$\frac{3}{7} \leq f_{LE}\vert_{r=a} \leq 1$	$\Lambda \leq e_{LE} \leq \Lambda\left(1+\frac{4}{3}\frac{\mathcal{F}_a}{\rho_a}\right)$
Bowers-Wilson	$\frac{1}{3} \leq f_{BW}\vert_{r=a} \leq 1$	$\Lambda \leq e_{BW} \leq \Lambda\left(1+2\frac{\mathcal{F}_a}{\rho_a}\right)$
Janka (Monte Carlo)	$0.39 \leq f_{MC}\vert_{r=a} \leq 1$	$\Lambda \leq e_{MC} \leq \Lambda\left(1+1.545\frac{\mathcal{F}_a}{\rho_a}\right)$
Maximum Packing	$\frac{1}{4} \leq f_{MP}\vert_{r=a} \leq 1$	$\Lambda \leq e_{MP} \leq \Lambda\left(1+3\frac{\mathcal{F}_a}{\rho_a}\right)$
Minerbo	$0.40 \leq f_{M}\vert_{r=a} \leq 1$	$\Lambda \leq e_{M} \leq \Lambda\left(1+1.488\frac{\mathcal{F}_a}{\rho_a}\right)$
Levermore-Pomraning	$f_{LP}\vert_{r=a} = 1$	$e_{LP} = \Lambda$

Table 2: Limits for the flux factors and the eccentricity for the different closure relations